BACHELOR

Determining the rate of dissipation of turbulent kinetic energy in the ocean

Meesen, A.R.G.

Award date:
2014

Determining the Rate of Dissipation of Turbulent Kinetic Energy in the Ocean

A.R.G. Meesen

June 2014
R-1841-S

Supervisors University of Western Australia:
Cynthia Bluteau, Nicole Jones and Gregory Ivey

Supervisor Eindhoven University of Technology:
GertJan van Heijst

Abstract

In this project a field data set collected on the Australian North West Shelf from the 5th until the 11th of April 2012 was processed, quality controlled, and analyzed. The focus was on the data collected at the BUBS station, data from other locations was analyzed only briefly. The ultimate goal of this project was to derive the rate of dissipation of turbulent kinetic energy (TKE), ϵ, from the turbulence velocity shear spectra. Using data obtained by two moorings nearby the final ϵ are described in the context of internal wave forcing. Various algorithms and techniques to estimate epsilon from velocity shear spectra were tested and evaluated to develop a methodology that can be used for future data analysis.

Two ways of estimating ϵ from the turbulence shear spectra were used, an integration method and a fitting method. In this project a computer program was used that uses both methods. The fitting method was developed in-house, the integration method used a code that came with the instrument. The values from the fitting method were used to interpret the data and draw conclusions. The program is designed so that every segment is checked manually and the range of fitted spectral observations can be modified when necessary. In total there are 7252 segments of which 2341 were rejected (32%). Of those segments 601 (8% of total) were rejected by the program and on top of that 1740 (24% of total) were rejected manually. This means that in the end 4911 (68%) good segments remained.

From the analysis of the program it followed that all ϵ values above 10^{-5} and below 10^{-9} W/kg can be rejected straight away and don't need to be checked manually. No correlation is found between the ϵ values that were rejected and the drop speed of the profiler. Therefore, all segments with an ϵ value between 10^{-9} and 10^{-5} W/kg should be checked manually. Another point is that the manually adjusted fits have a slight upward bias, which could be fixed by rewriting the code. However, the question is if that is worth the effort or if it is easier and quicker to just check these segments manually. Most of the accepted segments have a drop speed around 0.8 m/s. This is the most ideal drop speed, which is partly related to the characteristics of the sensors. When new casts are done, keeping the drop speed at 0.8 m/s for as long as possible is desirable.

The 24 hour epsilon profiles were described within the moored dataset, which has more temporal resolution. During this period two internal waves passed. The second one arrived 13.5 hours after the first, so the waves are out of phase with the dominant tidal period of 12.4 hours. The passing of internal waves has several effects on the water column. There are regions of high dissipation in well mixed regions close to the surface and these deepen as the internal wave passes and draws down the isotherms. Furthermore, the baroclinic velocities change rapidly with the passage of the internal waves, transporting cold water to the surface. Right after the internal wave passed there are really high values of dissipation measured near the seabed. This increase in ϵ was missed by the profiling.

Looking at the effects of internal waves, it is understandable that they have a great impact on heat and nutrient fluxes and can possibly damage offshore structures. Unfortunately, it is not possible to predict when and where the internal waves occur. They do not coincide with the tides and due to their high dissipative character it is hard to tell how far they will propagate. To understand the dynamics of internal waves better, more research is necessary to fill the gaps in the data.

Contents

Chapter 1

Introduction

As an applied physics student at Eindhoven University of Technology I went to Perth for a three month internship, from February till May 2014, at the Geophysical Fluid Dynamics group at the University of Western Australia. The research that is carried out there is focused on the coastal oceanographic area, mostly in Western Australia and aims at understanding ocean mixing as a result of internal waves. The results of this study will contribute to the sustainable development of the Australian North West Shelf (NWS). Information is urgently required to manage the conflicting uses of the NWS, which include oil and gas exploration and development, tourism and commercial fishing.

Internal waves can only exist in a stratified fluid, in lakes and oceans this happens when temperature and/or salinity changes with depth. In lakes internal waves are generated by wind, whereas in oceans internal waves occur when tides interact with a sloping topography. Internal tide generation plays a critical role in global ocean circulation, but because the phenomenon is ill understood it is hard to implement it effectively in global climate models. At a regional scale, nonlinear internal waves can induce near-bottom motions that drive significant turbulent mixing and cross-shore transport. This affects both horizontal and vertical fluxes of heat, nutrients and biological material. On the NWS nonlinear internal waves are probably important factors in the creation of ecological hotspots. In addition to such ecological effects, these energetic flows impact offshore structures and influence sediment mobilization and scour, affecting the stability of offshore structures and pipelines.

Current ocean circulation models use empirical parameterizations based on idealized engineering flows, obtained by either direct numerical simulations or laboratory work. The model flows are generated at much lower Reynolds numbers than in the field so their applicability remains to be demonstrated. To improve these model studies it is necessary to understand ocean mixing and transport of sediment in real flows and therefore field work is really important.

From the 5th to the 23rd of April 2012 data was collected by several moorings on the NWS. A mooring is a string of instruments attached to the sea floor. The moorings collected data like currents, temperature and pressure. From the 5th until the 11th of April profiles were taken at various sites on the NWS, see figures 1.1 and 1.2. A vertical microstructure profiler (VMP) was lowered to the bottom of the ocean and pulled back up, meanwhile collecting mean and turbulence data like temperature, pressure and velocity shear fluctuations. On the

10th and 11th of April regular VMP profiling took place at the BUBS site (latitude, longitude: -19.4383,115.9144) for 24 hours. Starting at 7 in the morning 5 or 6 profiles were done each hour, which took about 20 minutes (between 15 minutes past the hour and 15 minutes before the next hour). This project focused on the 123 profiles taken in this 24 hour period and I did a preliminary analysis of the VMP profiles collected at other sites.

The ultimate goal of this project was to determine the rate of dissipation of turbulent kinetic energy (TKE), ϵ, at the BUBS location. Using data obtained by two moorings nearby, the results were also related to the presence of internal waves. A program written by Cynthia Bluteau was used to get the ϵ values. Because it was the first time this program was used the output was evaluated, so that the program can be improved for use in future projects.

Figure 1.1: Location of the NWS on the map of Australia. See figure 1.2 for a detailed map of the locations of the casts.

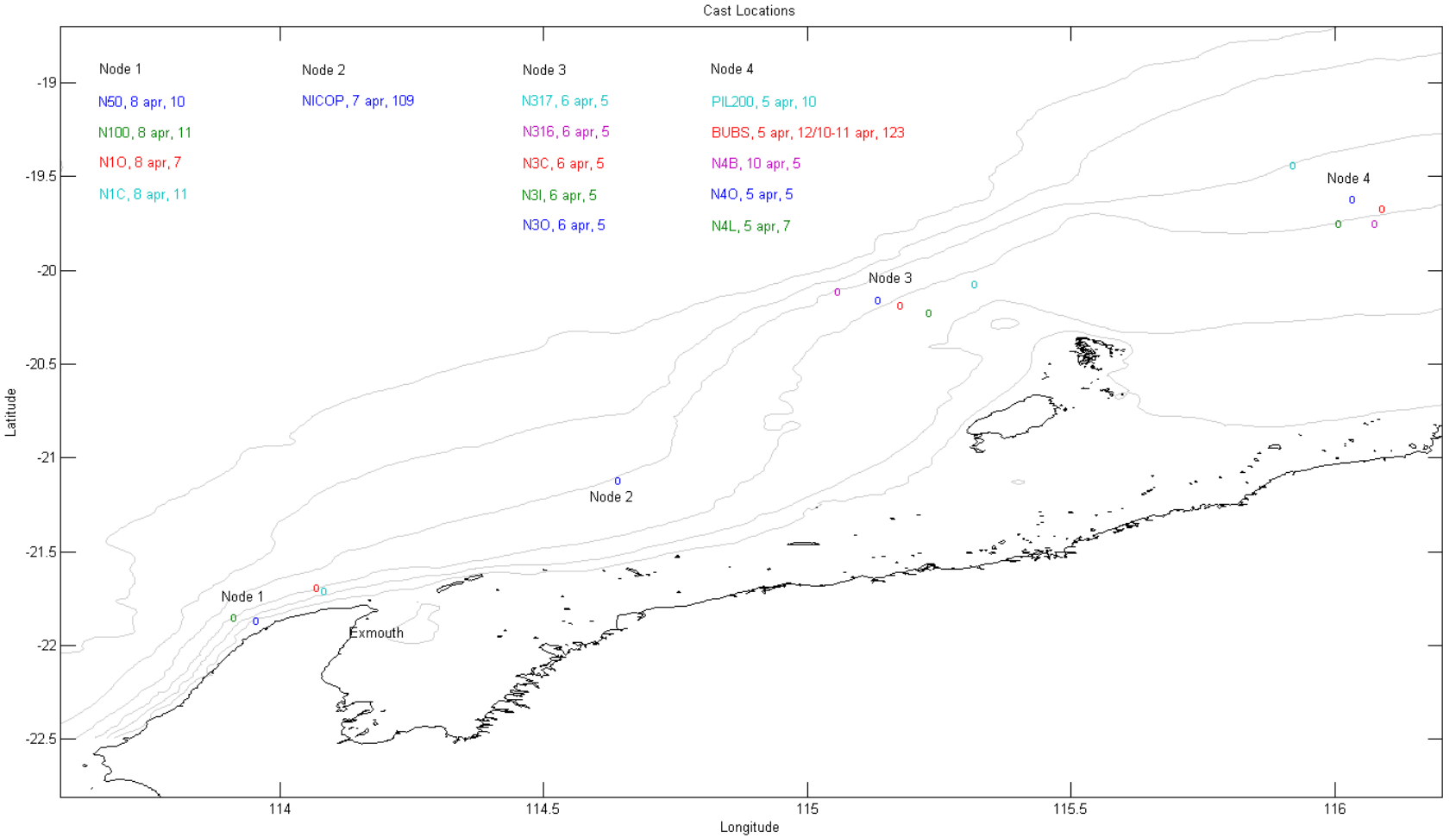

Figure 1.2: Locations where data was collected between the 5th and 11th of April 2012. After the date is the number of casts done at that location.

Chapter 2

Theory

To understand the collected data and the processing done on it one should be familiar with turbulence and the cascade of energy through turbulence. In this chapter the most important part of this project is explained, the velocity shear spectrum. The majority of the information in the section on the velocity shear spectrum was taken from the article by Lueck [2], but additional information is taken from other sources.

2.1 The velocity shear spectrum

When the largest eddies in a flow break into a cascade of smaller eddies, the TKE flows to ever smaller scales without any loss of energy. As the wave numbers increase, viscosity plays a more and more important role. Eventually, the energy is dissipated to heat through viscous dissipation. This scale of the smallest eddies should be of order

$$\eta = (\nu^3 \epsilon^{-1})^{1/4} \tag{2.1}$$

where ν is the kinematic molecular viscosity and ϵ is the rate of dissipation of turbulent kinetic energy. The part of the velocity spectrum for wave numbers comparable to and larger than η^{-1} is called the viscous range. The region where wave numbers are large compared to the energy-containing range and small compared to the dissipation range is usually called the 'inertial subrange', because the velocity fluctuations are unaffected by viscosity within this range of wave numbers.

The spectrum of the turbulent velocity fluctuations was first derived by Kolmogorov [4] under the assumption that the largest energy-containing scales of turbulence are much larger than the dissipative scales. The dissipation scale 2.1 is now commonly called the Kolmogorov scale. For the inertial subrange Kolmogorov showed that the velocity spectrum must be proportional to $k^{-5/3}$.

The form of the viscous part of the spectrum was not predicted by Kolmogorov. An empirical spectrum was derived by Nasmyth [5]. Oakey [6] formally published the Nasmyth empirical spectrum and also converted it into the spectrum of the rate-of-strain and shear, under the assumption of isotropic turbulence. The shear spectrum tabulated by Oakey is referred to as

the Nasmyth spectrum. Shear is the gradient of velocity, so this spectra rises in proportion to $k^{1/3}$ in the inertial subrange.

In isotropic turbulence the rate of dissipation of TKE is

$$\epsilon = \frac{15}{2}\nu\overline{\left(\frac{\partial u}{\partial z}\right)^2} = \frac{15}{2}\nu\int_0^\infty \Psi(k)dk \tag{2.2}$$

where Ψ is the spectrum of the shear $\partial u/\partial z$, the vertical gradient of the horizontal velocity u.

The non-dimensional form of the Nasmyth spectrum is tabulated at 13 different non-dimensional wavenumbers, $k\eta$, by Oakey [6] where k is in units of cycles per metre (cpm) and η is given by 2.1. This spectrum is shown in logarithmic coordinates in figure 2.1. The +1/3 (inertial subrange) is clearly visible, the ninth value is near the peak of the spectrum and for higher wavenumbers the spectrum drops rapidly due to dampening by molecular viscosity.

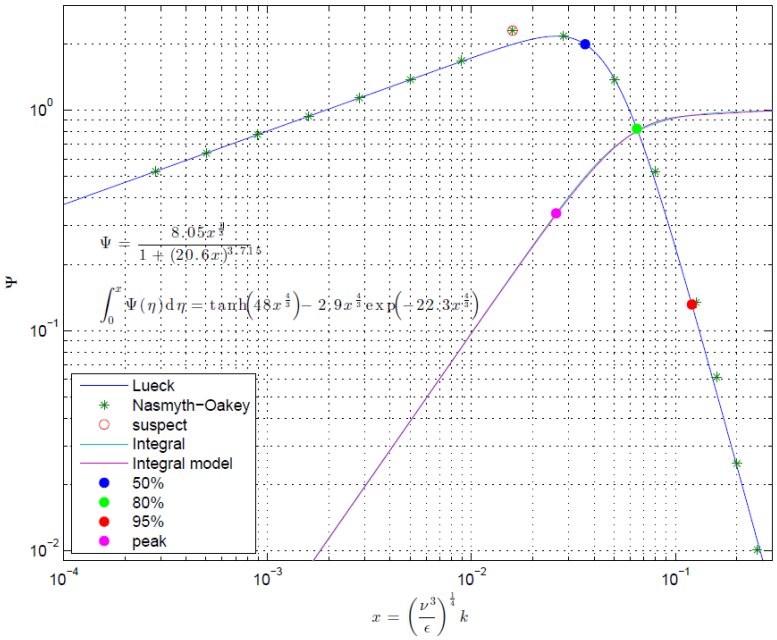

Figure 2.1: The non-dimensional Nasmyth empirical spectrum of shear (green asterisks) and its mathematical fit (blue). Fifteen-halves times the integral of the Nasmyth spectrum (cyan) and its mathematical fit (magenta). The points where the integral reaches 50, 80 and 95 % of its final value are indicated by blue, light-green and red circles, respectively. The peak of the spectrum is indicated by the magenta circle.

Wolk et al [7] provided a mathematical model of the Nasmyth spectrum, which is just a simple mathematical equation that fits well to the tabulated values of the Nasmyth spectrum. By definition, the integral of the non-dimensional shear spectrum, from zero to infinite wavenumber, must equal 2/15. The integral of the model is larger than this value by 4 %. This error has no practical consequences because there are other errors that are even bigger. Lueck has revised the model of Wolk slightly to bring the integral of the mathematical model of the Nasmyth spectrum to within 0.05 % of its expected value of 2/15. This model is the blue

curve in figure 2.1 and is given by

$$\Psi = \frac{8.05x^{1/3}}{1 + (20.6x)^{3.715}} \tag{2.3}$$

where $x = k\eta = k(\nu^3/\epsilon)^{1/4}$ and the wavenumber k is in units of cpm.

2.2 Richardson number

The Richardson number is defined as the square of of the Brunt-Vaisala frequency divided by the square of the velocity shear:

$$Ri = \frac{\frac{-g}{\rho_0}\frac{\partial \rho}{\partial z}}{(\frac{\partial u}{\partial z})^2} = \frac{N^2}{S^2} \tag{2.4}$$

in which g is the gravitational constant, ρ_0 is the density of the fluid parcel, ρ the density of the fluid around the parcel, u the velocity of the parcel and z the depth of the parcel.

The Richardson number is an indicator of the relative importance of mean velocity shear to mean stratification in a water column. Richardson numbers greater than 0.25 indicate that local stratification is large enough to suppress turbulence generation by velocity shear. Richardson numbers less than 0.25 indicate times and depths at which vertical mixing due to mean velocity shear could potentially occur.

2.3 Thorpe length scales

Thorpe length scales are used to characterize the size of the energy containing overturns, the largest turbulent eddies. The Thorpe length scales are estimated by identifying unstable overturns in the instantaneous vertical density profiles. The displacement d, the Thorpe displacement, of each density sample i is the distance a sample is moved adiabatically from the monotonic density profile [8]. The Thorpe length scales can be calculated by getting the root-mean-square of the Thorpe displacements [9]:

$$L_T = \left(\frac{1}{n} \sum_{i=1}^{n} d_i^2 \right) \tag{2.5}$$

In the field Thorpe length scales are calculated by temperature data collected by fast response temperature sensors. The resolvable size of the overturns is limited by the accuracy of the sensors and their vertical spacing. Temperature data is used because the density differences on the NWS arise from temperature differences. The salinity is constant as the NWS is deprived of fresh water.

Chapter 3

Methodology

This chapter explains the measurement technique that was used to collect the data and also the program that was used to analyze the data. Most of the information in the first section was taken from the article by Rolf Lueck [1].

3.1 Measurement technique

The data was collected with a VMP-500 microstructure turbulence profiler from the company Rockland Scientific. The instrument carries two shear probes, two fast-response temperature sensors (thermistors) and a number of other sensors, such as accelerometers, magnetometers and a pressure transducer. A graph and photo of the profiler can be seen in figure 3.1, the sensors are mounted on the bottom end. The motion sensors are placed at the middle of the instrument.

A VMP is deployed from a ship in a 'tethered free-fall mode' and is connected by a cable that is paid out fast enough to maintain 5 or 6 meters of slack near the surface. The fall speed is then fairly constant and independent of ship motions. During its descent to the bottom of the ocean data is collected (at 512 Hz for most sensors).

The fall speed of the profiler in this project was around 0.8 m/s for the mid-depth measurements. At the sea surface the speed was lower, because the profiler needs to gain speed. At the sea floor the speed was also lower, because hitting the sea floor too hard can damage the sensors.

In the end the results were compared to other data collected by two moorings also located at the 100 meter isobath. One was at the BUBS station, the other one a few hundred meters away. The BUBS mooring recorded high spatial and temporal resolution temperature and current measurements over the bottom 35 m of the water column, the other mooring recorded over a depth of 80 meters.

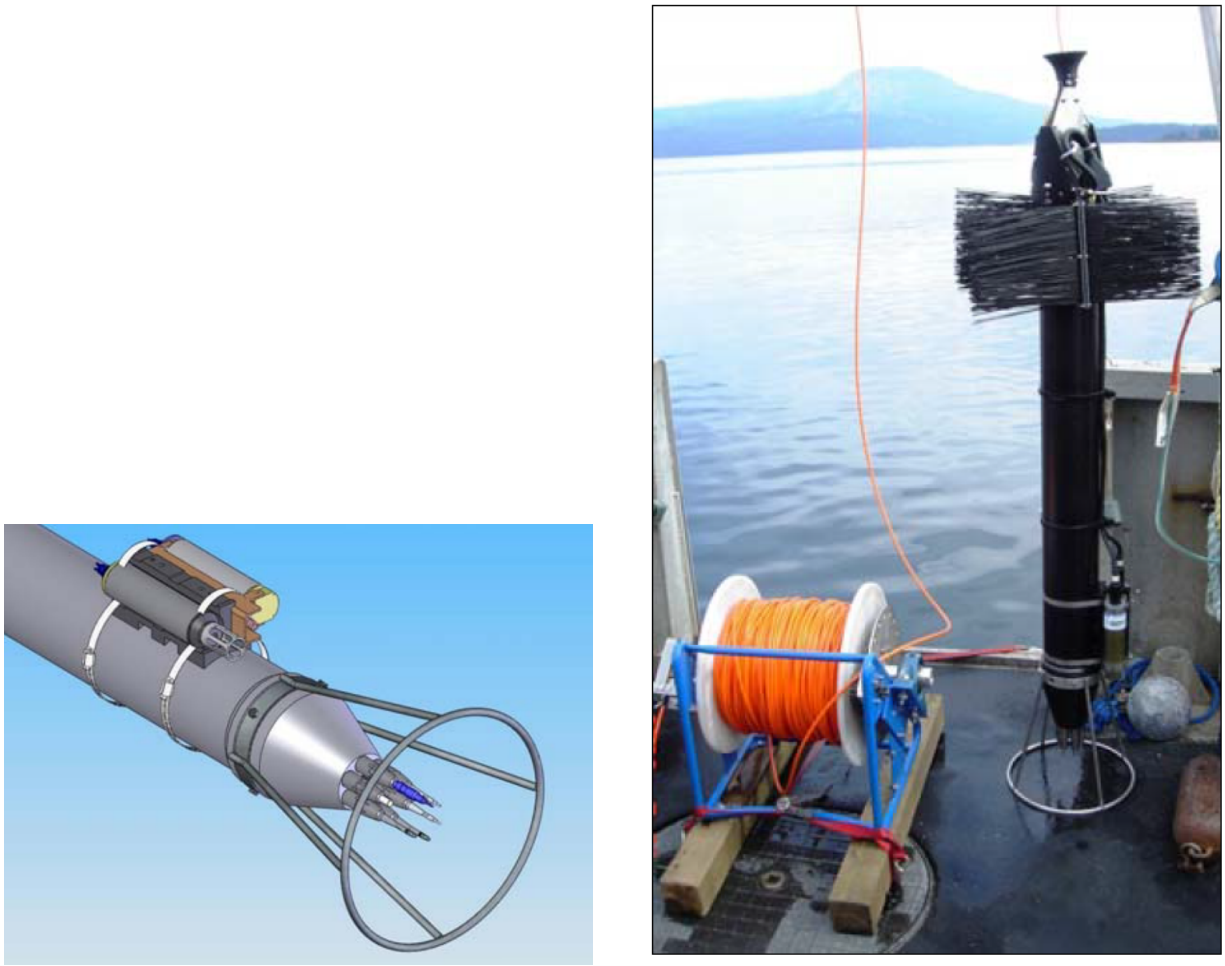

Figure 3.1: The VMP-500 profiler with its sensors and a cage protecting the sensors once the profiler hits the sea floor.

3.2 Data analysis

To get an estimate of ϵ the shear spectrum was used. First, every profile was divided into segments of 2048 points, with each segment overlapping the previous one by 50%. These segments were then divided into four blocks and a Fast Fourier Transform was applied to each one to get the power spectral density. The four blocks were then averaged to get a spectra of the corresponding segment. With the profiler falling at a velocity of about 0.8 m/s and a sampling frequency of 512 Hz, 2048 points corresponds to a segment length of about 3 meters. This means that for every profile around 60 estimates of the rate of dissipation were calculated.

There are two ways of estimating ϵ from the collected data, an integration method and a fitting method. In this project a program was used that uses both methods, but the values from the fitting method were used to interpret the data and draw conclusions.

The integration method integrates under the graph (see equation 2.2) to get a first guess of ϵ and then refines this guess as well as possible. The wave number limits are calculated

by comparing the Nasmyth spectrum against the measured spectrum for non-dimensional wavenumbers up to 0.04, which is just above the spectral maximum. The lower limit is at 10 cpm, the upper limit starts at a point slightly higher than the spectral maximum. If the measured spectrum is consistently above the nasmyth spectrum, the upper limit of integration is increased, otherwise it is decreased. The range is always between 10 cpm and 150 cpm. The estimates of ϵ can be used to estimate the fraction of the variance that is resolved (the circles in figure 2.1), then the estimate can be adjusted to account for the missing variance.

The fitting method used a maximum likelihood estimator to account for the χ-distributed nature of spectral observations to fit the Nasmyth spectrum to the observed shear spectrum. Since the Nasmyth spectrum covers both the inertial and viscous range (see figure 2.1), the technique can be applied to the inertial subrange. The drawback of this method is that if the noise-dominated wavenumbers are included in the fit, the estimated epsilon is biased by the larger number of spectral observations contained in the noise (high-frequency) portion of the spectra. To identify the range over which to fit, a third order polynomial was fitted to the spectrum to identify the local dip in the spectrum that occurs just before the noise starts to dominate. This local minimum was set as K_{max} and was used for the fit. If this point lay beyond the point where 80% of the variance of the dissipation range is contained, K_{max} was set to k_{80}.

At the bottom of each profile the drop speed slows. All segments with a drop speed below 0.1 m/s were not analysed. This is because when the drop speed is too low, the signal to noise ratio of the data is too low.

Chapter 4

Results and discussion

In this chapter the results are discussed, which are divided into three categories. First the quality of the data is presented, then the analysis of the program and finally the ϵ values are presented, along with data collected by the two moorings.

4.1 Data quality control

Before starting the calculations of ϵ, the quality of the data was checked on several points. This is done to make sure all the casts were performed right and to make sure the conversion from raw data into physical units was successful.

4.1.1 Profile duration

The duration of each profile was calculated and plotted in figure 4.1. Three profiles are much shorter than the others, number 1, 3 and 18. These casts didn't go as planned and were aborted before the profiler reached the sea floor.

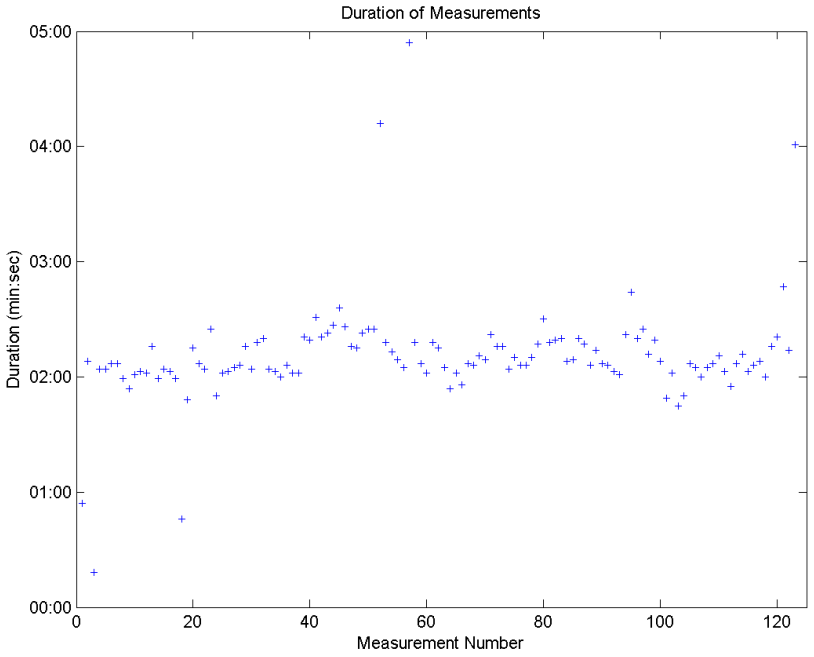

Figure 4.1: Duration of all the measurements, it is clear that number 1, 3 and 18 were aborted.

4.1.2 Temperature

The temperature data was checked and edited on several points, but because it was not used for any conclusion this process is placed in appendix A.

4.1.3 Heading, pitch and roll

The heading, pitch and roll of the instrument indicate if the profiler spins around its axis and if it remains vertical during the measurements. The heading indicates in which direction the horizontal axis is pointing, with 0° corresponding to north, 90° to east, 180° to south and 270° to west. The pitch and roll indicate how much the instrument is tilted from the vertical axes into the horizontal planes.

In figures 4.2 to 4.4 these measurements are displayed, it is clear that the profiler did not spin very much and it was also almost perfectly vertical during all the measurements. For visual clarity, the gradient of the heading is plotted.

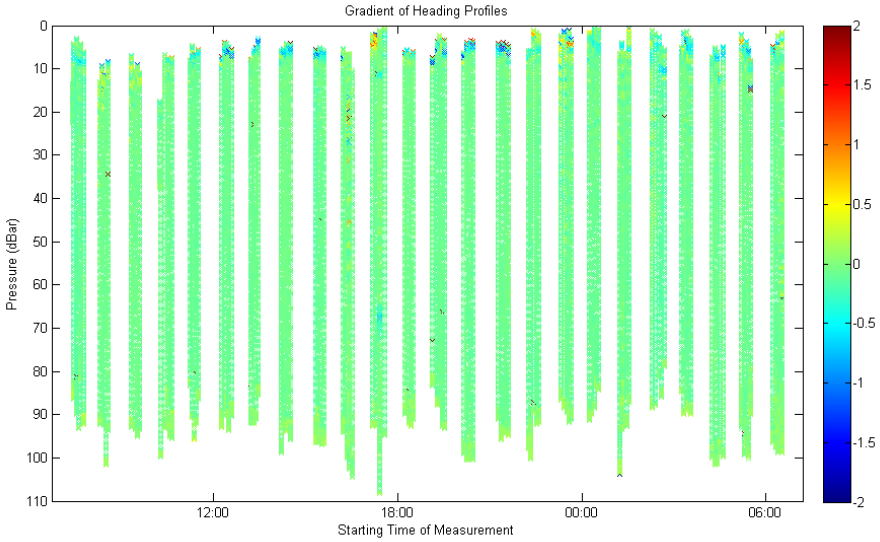

Figure 4.2: The difference in heading in degrees between subsequent profiles. Since this difference stays close to zero in almost the whole graph, this means that the profiler did not change its heading quickly.

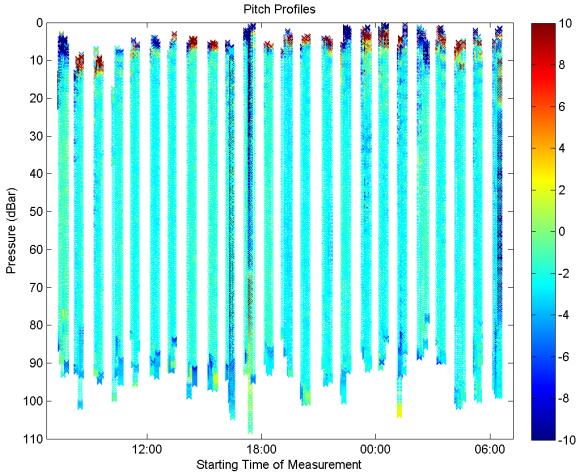

Figure 4.3: The pitch of the profiler. The colors represent the degrees the profiler is tilted around its horizontal axis. The pitch stayed within +/- 2 degrees in almost the whole graph, this means that the profiler was moving vertically.

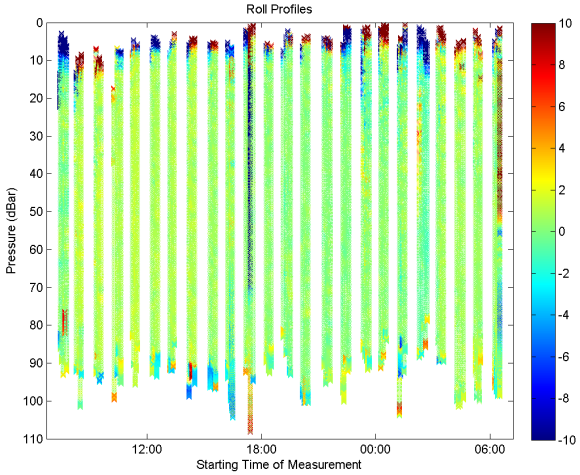

Figure 4.4: The roll of the profiler. The colors represent the degrees the profiler is tilted around its horizontal axis. The roll stayed within +/- 1 degree in almost the whole graph, this means that the profiler was moving vertically.

4.2 Program analysis

In this section the analysis of the program used to calculate the ϵ values is presented. It is the first time it was used, so this analysis will help to improve it for use in future projects.

4.2.1 Fitting the results

An example of two segments can be seen in figure 4.5. There were two shear probes on the profiler, the green and blue curves. The solid curves are the solution from the integration method, the dashed lines are from the fitting method. The dashed gray curves in the background are the theoretical Nasmyth spectra for different ϵ, the color bar shows which ϵ belongs to which curve, -7 means that $\epsilon = 10^{-7}$. The orange and red curves are used by the algorithm to estimate the minimum in the curves right before the noise starts.

In order to get the fits to all the segments as well as possible, the fits were manually checked and the maximum wavenumber fitted (K_{max}, ∇ in figure 4.5) was adjusted if necessary. If the data of a certain segment was really bad, as in the right one in figure 4.5, the ϵ estimates were rejected. Sometimes just a slight modification was necessary, this is displayed in figure 4.6. The left graph shows the segment without visual control, the right one shows it after manually adjusting the fit. It can be seen in this figure that both K_{max} values were increased, which also increased the ϵ values.

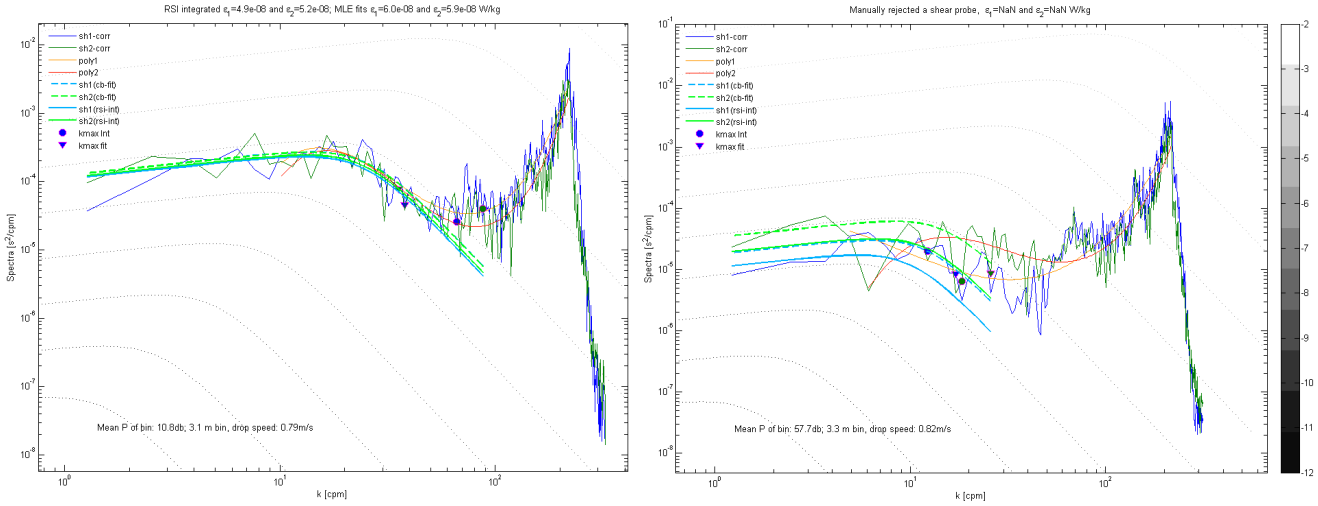

Figure 4.5: An example of two segments of a profile fitted with a Nasmyth spectrum. The left segment is an example of a segment where the program worked really well. The left segment is manually rejected, because the shape of the Nasmyth spectrum can not be distinguished in this graph.

4.2.2 Before and after visual quality control

In figures 4.7 and 4.8 the result of all the fits on all profiles is displayed, first the results without doing any visual quality control and second the results after the visual quality control. From these two graphs it is clear that the highest and lowest values of ϵ were rejected when manually checked, an example of this was displayed before in figure 4.5.

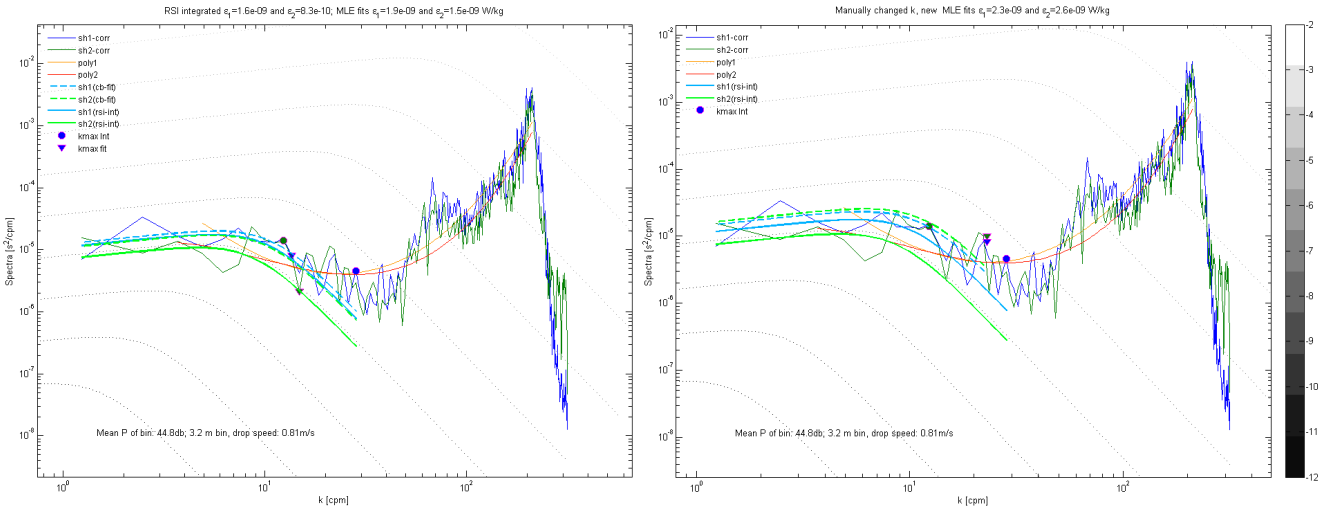

Figure 4.6: An example of two segments of a profile fitted with a Nasmyth spectrum. The left graph shows the fits done by the program. The right segment is manually changed by changing the k_{max}. The k_{max} in the right graph is higher for both probes. This also increases both ϵ values, from 1.9 and 1.5 to 2.3 and 2.6 (10^{-9} W/kg).

In total there are 7252 segments of which 2341 were rejected (32%). Of those segments 601 (8% of total) were rejected by the program and on top of that 1740 (24% of total) were rejected manually. This means that in the end 4911 (68%) good segments remained. In table 4.1 the percentage of rejected segments for each ϵ range is displayed.

ϵ range	segments before QC	rejected segments	percentage rejected
$\epsilon < 10^{-9}$	198	182	92
$10^{-9} < \epsilon < 10^{-8}$	1984	896	45
$10^{-8} < \epsilon < 10^{-7}$	2721	300	11
$10^{-7} < \epsilon < 10^{-6}$	1448	161	11
$10^{-6} < \epsilon < 10^{-5}$	189	92	49
$10^{-5} < \epsilon < 10^{-4}$	62	61	98
$10^{-4} < \epsilon < 10^{-3}$	45	45	100
$10^{-3} < \epsilon < 10^{-2}$	4	4	100

Table 4.1: Percentage of rejected segments per ϵ range.

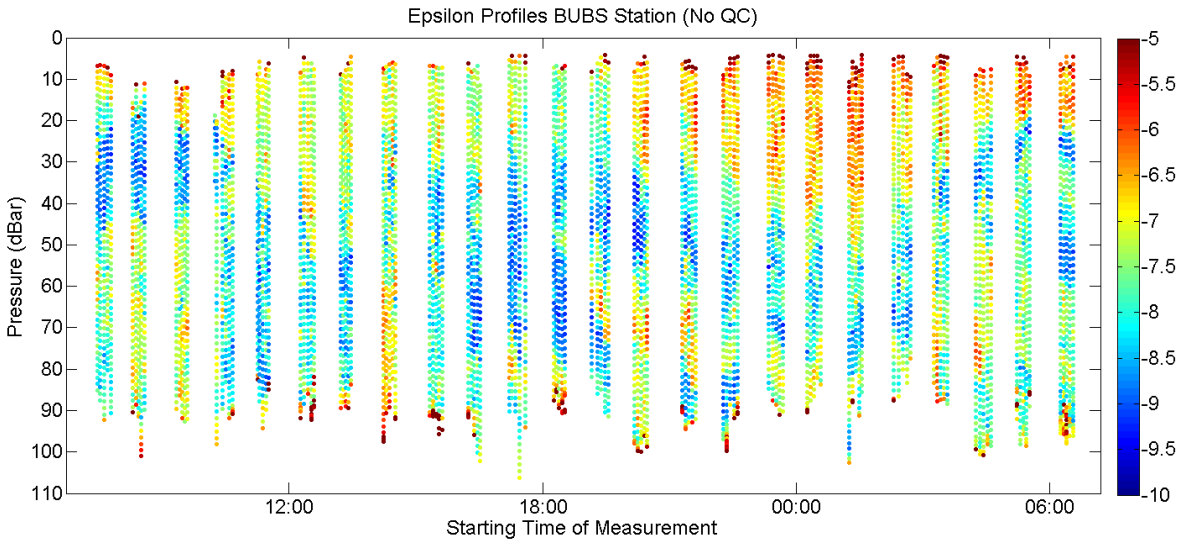

Figure 4.7: Calculated ϵ values for all profiles by fitting the Nasmyth spectrum to the results without visual quality control. The colorbar gives $^{10}log(\epsilon)$. The mean value of the two shear probes is presented here. The measurements were done in timezone UTC +8 on the 10th and 11th of April 2012.

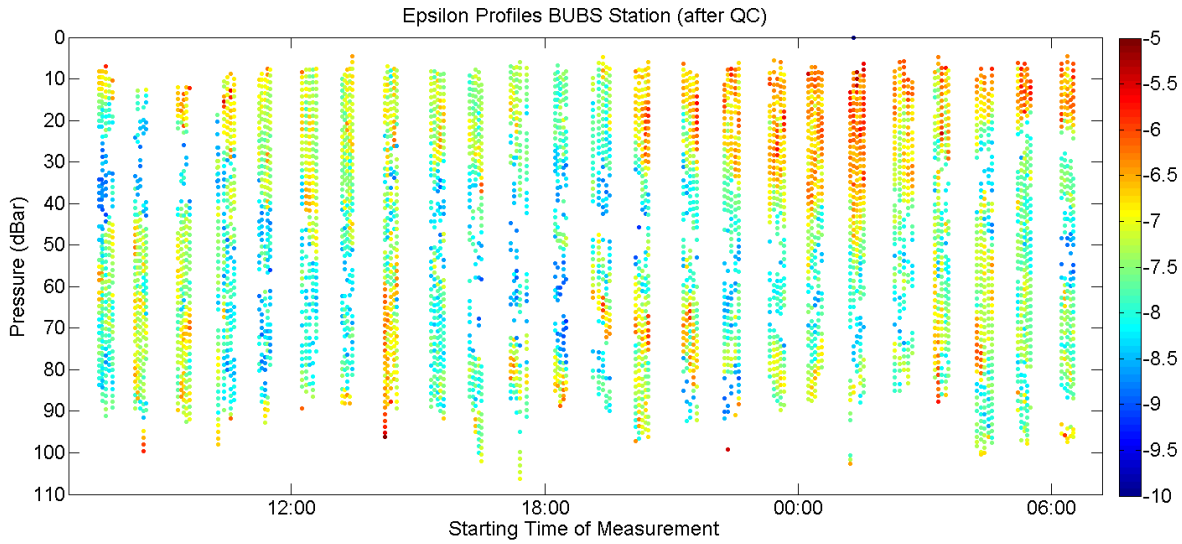

Figure 4.8: The same results as in figure 4.7, but now after the visual quality control.

In figure 4.9 the data before and after the manual check is plotted against each other. Obviously, mostly the high and low ϵ values were rejected. Manually changing K_{max} in the range -9 to -7 results in an upward bias in ϵ. In almost every profile there were a number of segments that looked like the program's fit was too low. An example of this was already given in figure 4.6. The reason for this is probably that the code that tries to find the dip in the data before the noise starts does not work well in the ϵ-range between 10^{-9} to 10^{-7}.

In figures 4.10 and 4.11 two histograms are displayed. The median of the data after quality control is increased, which confirms the slight bias in figure 4.9. It is also clear again that the really high values in particular were rejected by the visual control.

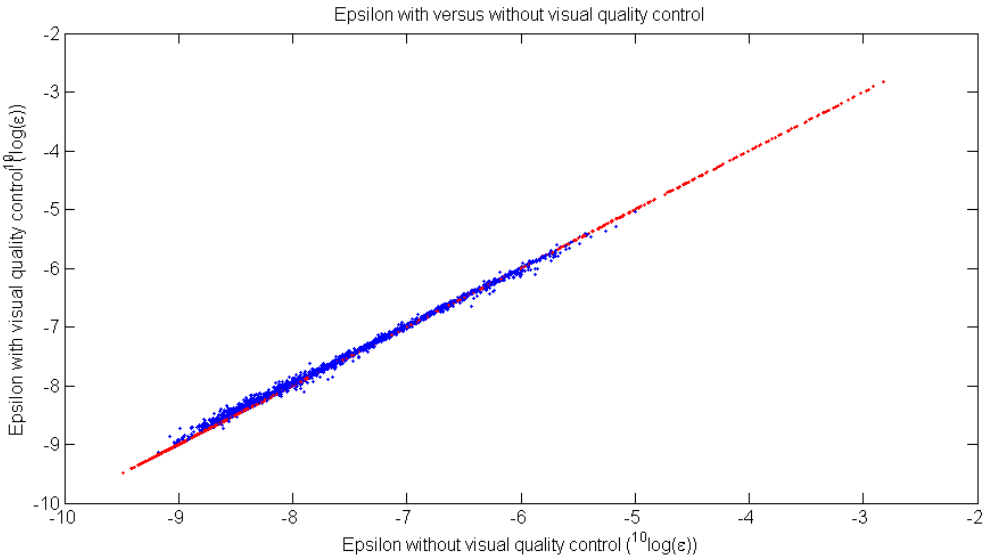

Figure 4.9: Plot of all the data, where on the x-axis the data before the visual check is displayed and on the y-axis the data after the visual check. The red dots are the segments where the program found a value but this value is rejected manually.

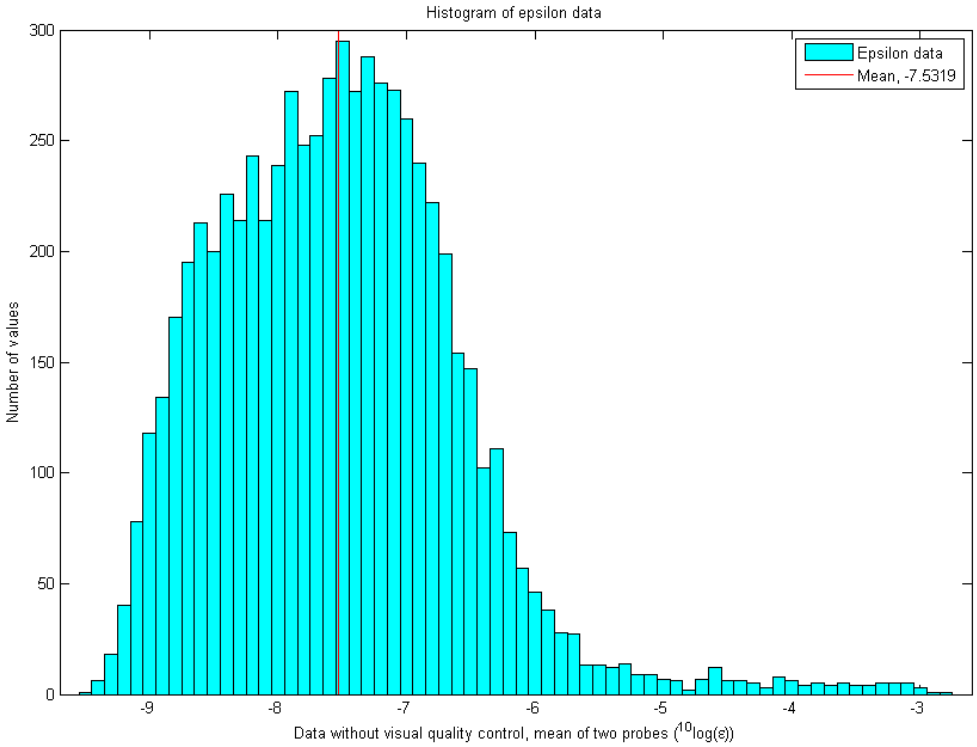

Figure 4.10: Histogram of the data without the visual quality control.

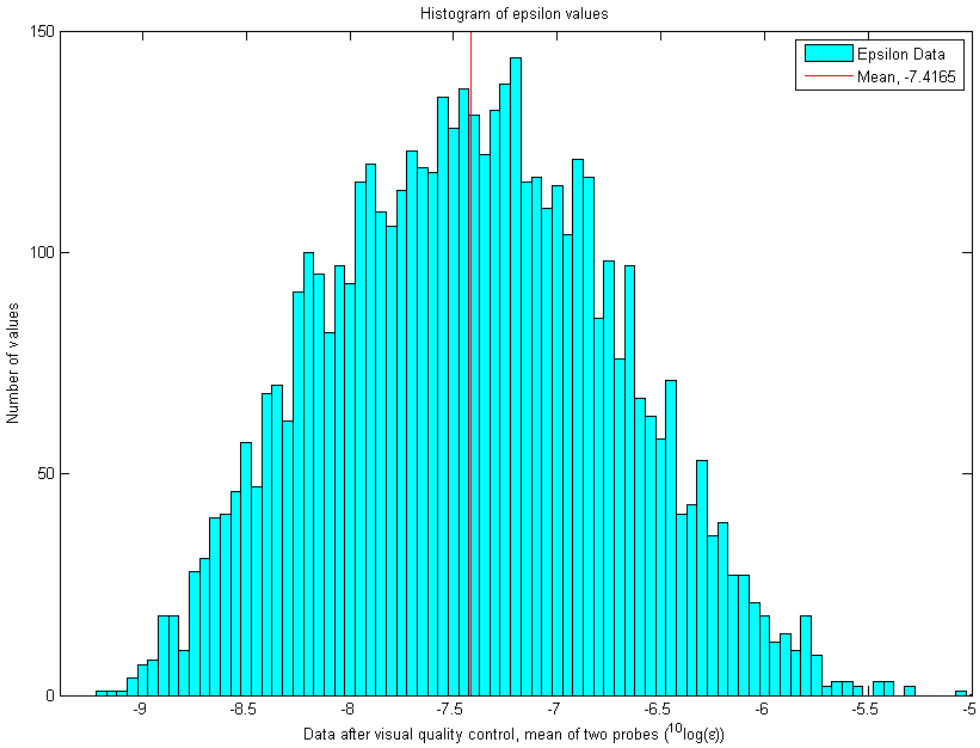

Figure 4.11: Histogram of the data after the visual quality control.

4.2.3 Drop speed

To see if there is a correlation between the drop speed and the accepted segments, a lot of graphs were made. In figure 4.12 the manually rejected values (the red points in figure 4.9) are plotted again, the color of the dots represents the drop speed of the profiler. In figure 4.13 the accepted values are plotted, where the color of the dots again represents the drop speed. In appendix B histograms of the drop speed of the rejected values are displayed. In table 4.2 the percentage of rejected segments in each drop speed range is displayed.

drop speed range (m/s)	segments before QC	rejected segments	percentage rejected
0 - 0.1	1	0	0
0.1 - 0.2	256	14	5
0.2 - 0.3	174	58	33
0.3 - 0.4	118	54	46
0.4 - 0.5	104	47	45
0.5 - 0.6	112	51	46
0.6 - 0.7	307	118	38
0.7 - 0.8	3229	718	22
0.8 - 0.9	2860	664	23
0.9 - 1.0	1	1	100

Table 4.2: Percentage of rejected segments per drop speed range.

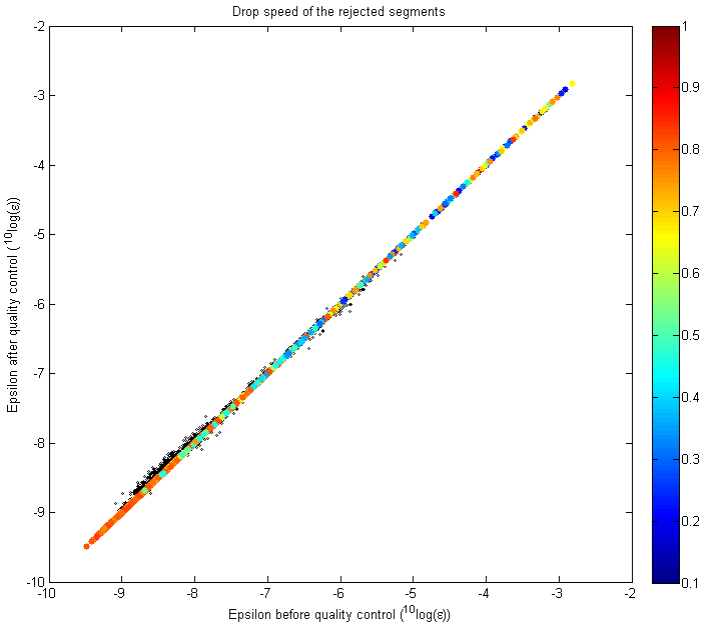

Figure 4.12: Plot of the manually rejected data (red points in figure 4.9), the color represents the drop speed of the profiler. The black points are the accepted segments.

In figures 4.13 and B.1 it can be seen that most of the accepted segments have a drop speed around 0.8 m/s. The mean and median drop speed of the accepted segments are respectively 0.78 and 0.80 m/s. It is surprising that even though 0.8 m/s was the typical drop speed, a large percentage of the segments with a lower drop speed were accepted, see table 4.2.

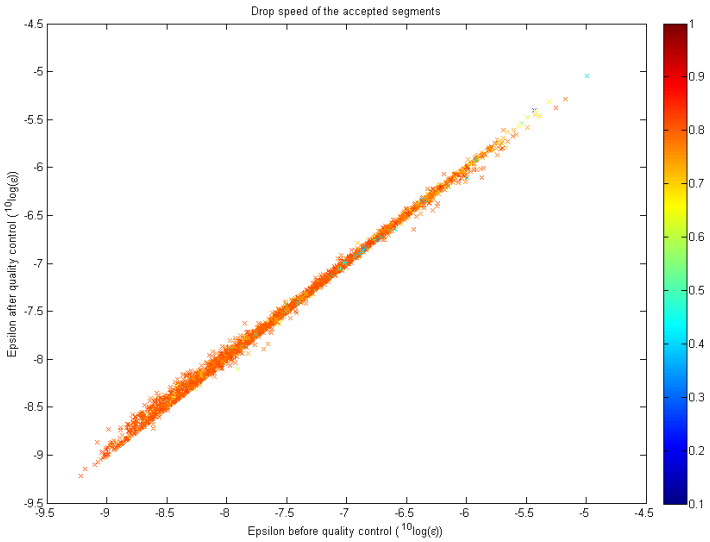

Figure 4.13: Plot of the accepted data, the color represents the drop speed of the profiler.

4.3 Final results

This section presents the final results of the rate of dissipation of TKE at the BUBS location in the context of data collected by the two moorings. An overview of ϵ results from processing the VMP profiles at the other locations can be found in appendix C.

The results of the casts done at the BUBS location on the 10th and 11th of April are displayed in figures 4.14 and 4.15, along with other data collected by the moorings. In figure 4.14 the first 12 hours are displayed and the last 12 hours in figure 4.15. Panel 1 to 4 in each of the graphs comes from the BUBS location. The 5th panel is data collected by a mooring that is located a few hundred meters away.

The black lines in the first panels are the isotherms, the colored lines are the resolved Thorpe length scales. They were only calculated for the bottom 30 meters, because that is where the thermistors are situated. The third panels display the ϵ estimates after visual control of the fitting method. The last two panels in each of the figures display the temperature in colors. The arrows give the baroclinic velocity of the water, which is the measured velocity minus the depth-averaged velocity. Arrows pointing to the right correspond to inshore velocities and arrows pointing to the left to offshore velocities.

The second panels give $^{10}\log(\frac{Ri}{Ri_{cr}})$, where Ri_{cr} is the critical Richardson number. Dark blue corresponds to numbers below zero, which means below the critical value. The dark blue parts is where shear is dominant over stratification, values above zero correspond to stable conditions. White values are unresolved, because N^2 is unstable in those places.

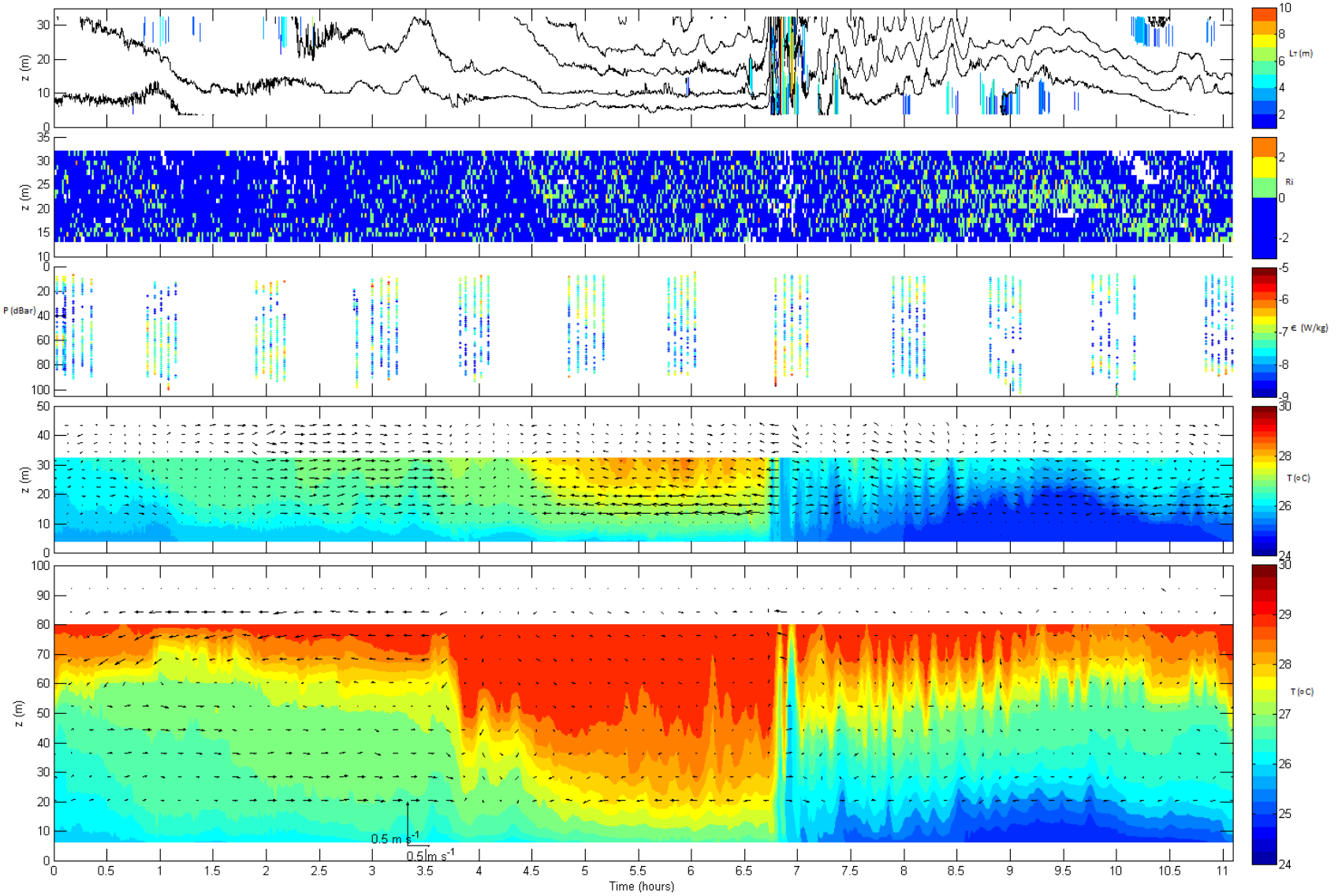

Figure 4.14: Results from the first 12 hours collected at the BUBS location, either by a VMP or a mooring.

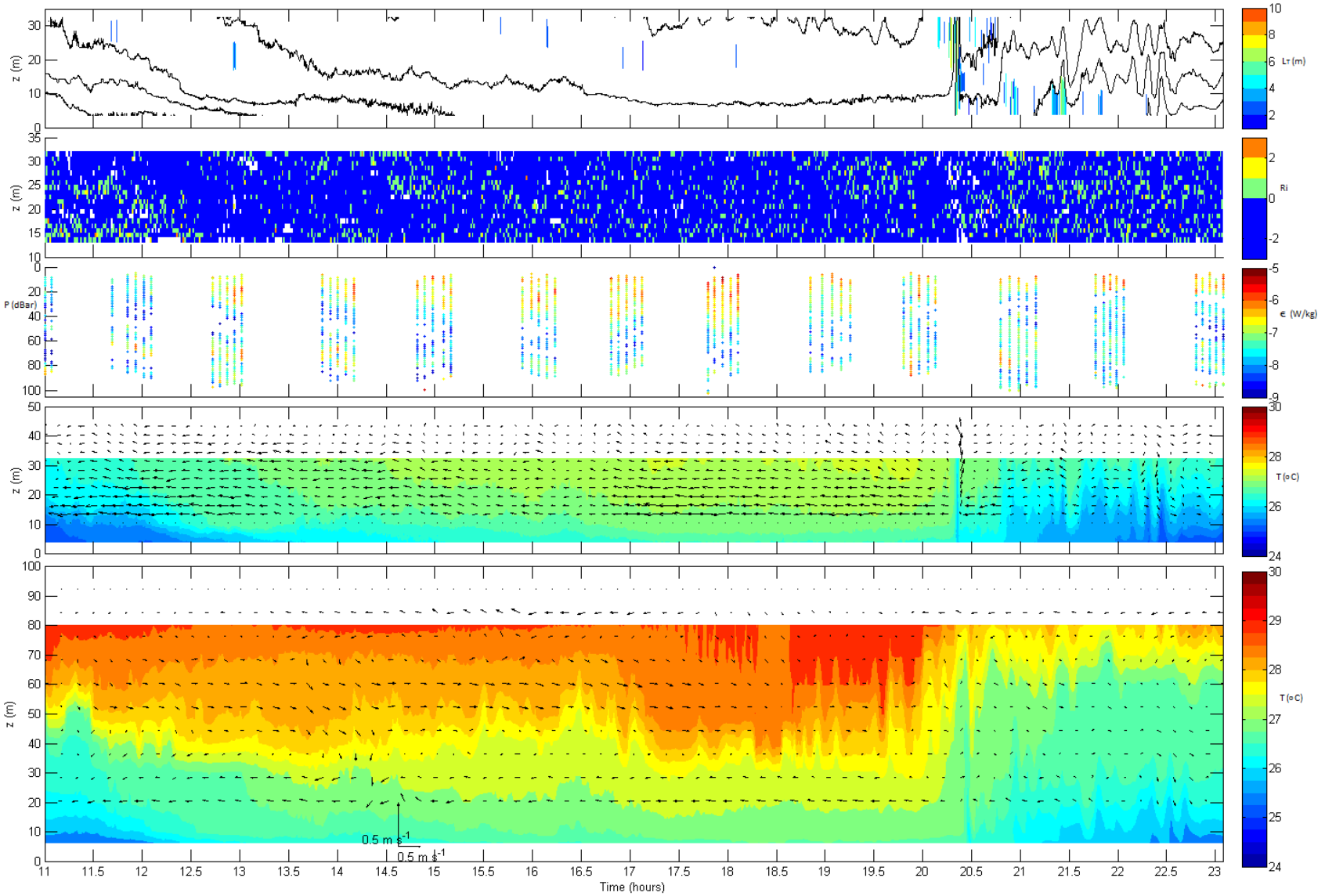

Figure 4.15: Results from the last 12 hours collected at the BUBS location, either by a VMP or a mooring.

It's very clear that during the 24 hours that the measurements were done, two internal waves passed. On is really distinctive from 3.5 to 7 hours, the other one is a bit longer and less clear, it goes from 11.5 to 20.5 hours. The two waves were not in phase with the semidiurnal tide (12.4 hour period), the second one arrived 13.5 hours after the first one.

With the first internal wave the temperature started to drop from 3.5 hours. Just before the seventh hour the tail reached the BUBS location and caused cold water to be swept up to the surface very suddenly. This also caused an oscillation in the temperature. There is also a sudden change in the baroclinic velocities. They change from offshore to inshore in only a few minutes. Another thing that happened is that the dissipation at the sea floor increased rapidly. Between 3.5 and 6.5 hours the highest dissipation values were at the surface, but just before the seventh hour really high values appeared near the seabed. The last thing that stands out is that the Thorpe length scales are high right after the internal wave passed.

The same things happened when the second internal wave passed, but they are all a bit less distinct. First, the temperature dropped gradually and just before 20.5 hours cold water was swept up suddenly. Then an oscillation is visible in the temperature. The baroclinic velocities changed rapidly, they were directed upwards, which indicates that water from the bottom was being transported to the surface. The high Thorpe length scales are also visible after this internal wave passed. Unfortunately, the rise in dissipation at the seabed can not be seen with this internal wave, because no casts were done at that time.

Most of the time the Richardson number is smaller than zero, which means that the conditions are right for vertical mixing to occur. It does look like the Richardson number is higher in the time frame from 8 to 11.5 hours. The dissipation rates are low or not even measurable during this period. This indicates that during this period the stratification of the water column is stronger than the shear and is preventing vertical mixing from happening.

Chapter 5

Conclusions

The conclusions are divided into two parts. The first part is on the program that was used, since this was the first time it was used, some recommendations for future use are presented here. The second part is on the ϵ estimates in relation to the data collected by the two moorings.

5.1 Program

When looking at figure 4.9 and table 4.1, a logical conclusion is that all ϵ values above 10^{-5} and below 10^{-9} W/kg can be rejected straight away and don't need to be checked manually. Another criterion on which segments could be eliminated is the drop speed, but from figure 4.12, table 4.2 and the histograms in appendix B no correlation can be seen between the ϵ values that were rejected and the drop speed of the profiler.

Right now the minimum drop speed is set to 0.1 m/s and from these results there is no justification for increasing it. Therefore, all segments with an ϵ value between 10^{-9} and 10^{-5} W/kg should be checked manually.

The slight upward bias in figure 4.9 could be fixed by rewriting the code to get it to better estimate the dip in the data right before the noise. However, the question is if that is worth the effort or if it is easier and quicker to just check these segments manually.

From figure 4.13 it is clear that most of the accepted segments have a drop speed around 0.8 m/s and from table 4.2 it can be seen that the least segments are rejected between 0.7 and 0.9 m/s. The mean and median drop speed of the accepted segments are respectively 0.78 and 0.80 m/s. This means that when new casts are done, keeping the drop speed at 0.8 m/s for as long as possible will probably improve the quality of the data.

5.2 Dissipation

The passing of internal waves has several effects on the water column. There are regions of high dissipation in well mixed regions close to the surface and these deepen as the internal wave passes and draws down the isotherms. Furthermore, the baroclinic velocities change

rapidly, transporting cold water to the surface and right after the internal wave passed there are really high values of dissipation measured near the seabed.

Looking at the effects of internal waves, it is understandable that they have a great impact on heat and nutrient fluxes and can possibly damage offshore structures. Unfortunately, it is not possible to predict when and where the internal waves occur. They do not coincide with the tides and due to their high dissipative character it is hard to tell how far they will propagate.

To understand the dynamics of internal waves better, more research is necessary to fill the gaps in the data. In this data set there were five or six casts done every hour. However, the problem is that these five casts were done in half an hour and after that there is a gap of half an hour before the next casts started.In this data set important information is missing because right at a crucial point, when the second internal wave arrived at the site, no casts were done.

Bibliography

[1] *Measuring Tidal Channel Turbulence with a Vertical Microstructure Profiler (VMP)*, Rolf Lueck, Fabian Wolk and Kevin Black, Rockland Scientific International Inc., Victoria, BC, Canada, 2013

[2] *Calculating the Rate of Dissipation of Turbulent Kinetic Energy*, Rolf Lueck, Rockland Scientific International Inc., Victoria, BC, Canada, 2013

[3] *A First Course in Turbulence*, H. Tennekes and J.L. Lumley, MIT Press, 1989

[4] *Local structure of turbulence in an incompressible fluid at very high Reynolds number*, A.N. Kolmogorov, Doklady AN SSSR, 4:299-303, 1941

[5] *Ocean Turbulence*, P.W. Nasmyth, PhD thesis, University of British Columbia, Vancouver, British Columbia, Canada, 1970

[6] *Determination of the rate of dissipation of turbulent kinetic energy from simultaneous temperature and velocity shear microstructure measurements*, N.S. Oakey, Journal of Physical Ocianography, 12:256-271, 1982

[7] *A new free-fall profiler for measuring bio-physical microstructure*, F. Wolk, H. Yamazaki, L. Seuront and R.G. Lueck, Journal of Atmospheric and Oceanic Technology, 19:780-793,2002

[8] *Turbulence and Mixing in a Scottish Loch*, S.A. Thorpe, Philosophical Transactions of the Royal Society of London. Series A, Mathematical and Physical Sciences, vol. 286, no. 1334, pp. 125-181, 1977

[9] *Vertical overturns: A comparison of Thorpe and Ozmidov length scales*, T.M. Dillon, Journal of Geophysical Research, 87, 9601-9613,1982

Appendix A

Processing of temperature data

The temperature of the water was measured with two sensors. A Sea-Bird thermometer to measure the mean temperature and a fast-response thermistor probe to measure the turbulence temperature fluctuations. The lowest temperature that was measured is 24.54°C and the highest is 29.17°C.

In figure A.1 the data from the Sea-Bird thermometes is displayed, it is clear that there are a lot of spikes. In figure A.2 the data is displayed after all the spikes are removed. In some profiles a lot of information is lost because of this.

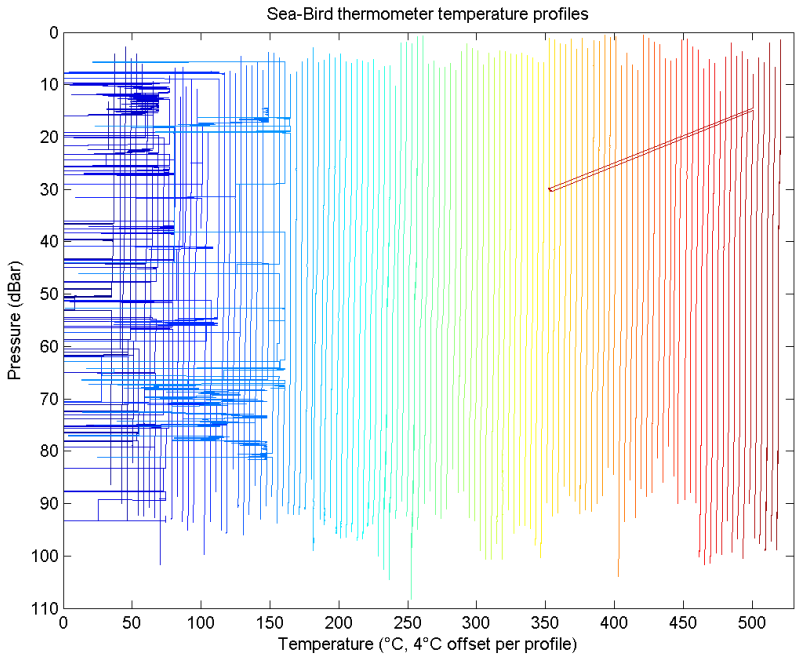

Figure A.1: All 123 temperature profiles measured with the Sea-Bird thermometer. Each profile has a different color and a 4° C offset with respect to the previous one. It is clear that a lot of the profiles have chunks of wrong data.

The temperature measured with the thermistor probe is displayed in figure A.3. Here, the data

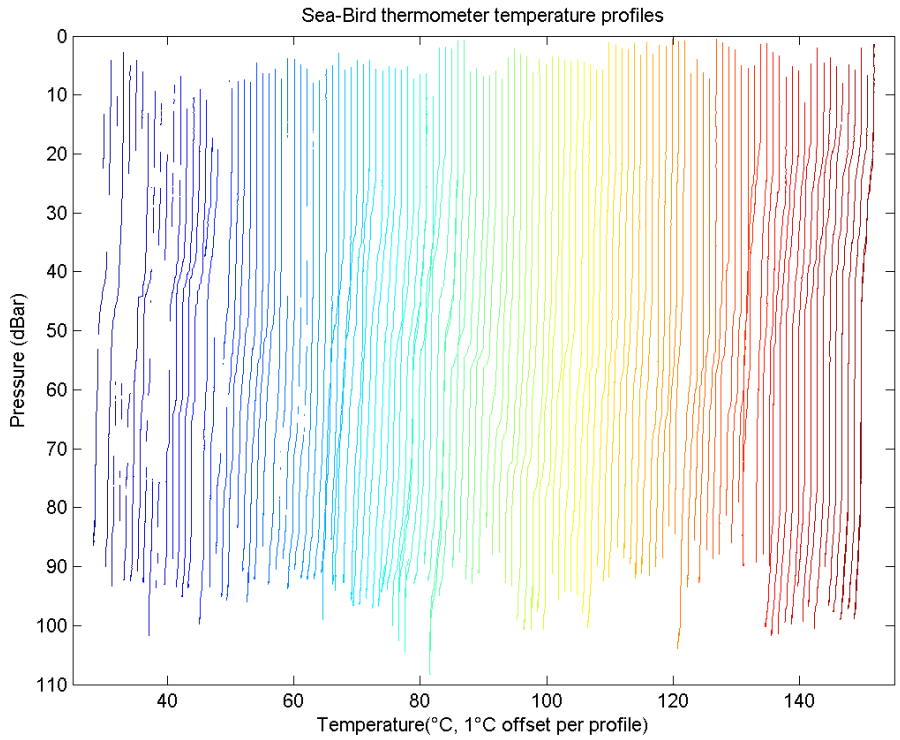

Figure A.2: The same temperature profiles as in figure A.1, but now with the erroneous data removed.

is represented in a different way, the profiles are ordered according to the starting time of the measurement and the colors indicate the measured temperature. This sensor is conditioned to provide really good spectra, but not a good mean value of the temperature. The mean temperature measured by this sensor has an offset with respect to the temperature measured by the Sea-Bird thermometer, this can be seen in figure A.4. The red line in figure A.4 is a fit of the data, the equation of the fit, with TP temperature the temperature measured by the thermistor probe and SB temperature the temperature measured with the Sea-Bird thermometer:

$$TP\ temperature = 0.91 \cdot (SB\ temperature) - 2.18. \tag{A.1}$$

To determine at what depths mixing plays an important role, the temperature gradient is investigated. In figure A.5 an example of the temperature gradient of profile number 16 can be seen. To be able to distinguish some difference in the gradient over the depth, all gradients higher than $3°C/$m or lower than -$3°C/$m were deleted first. The gradients at the top and at the bottom were so high that the other gradients were not visible anymore. It is clear now that there are patches with higher gradients and patches with lower gradients.

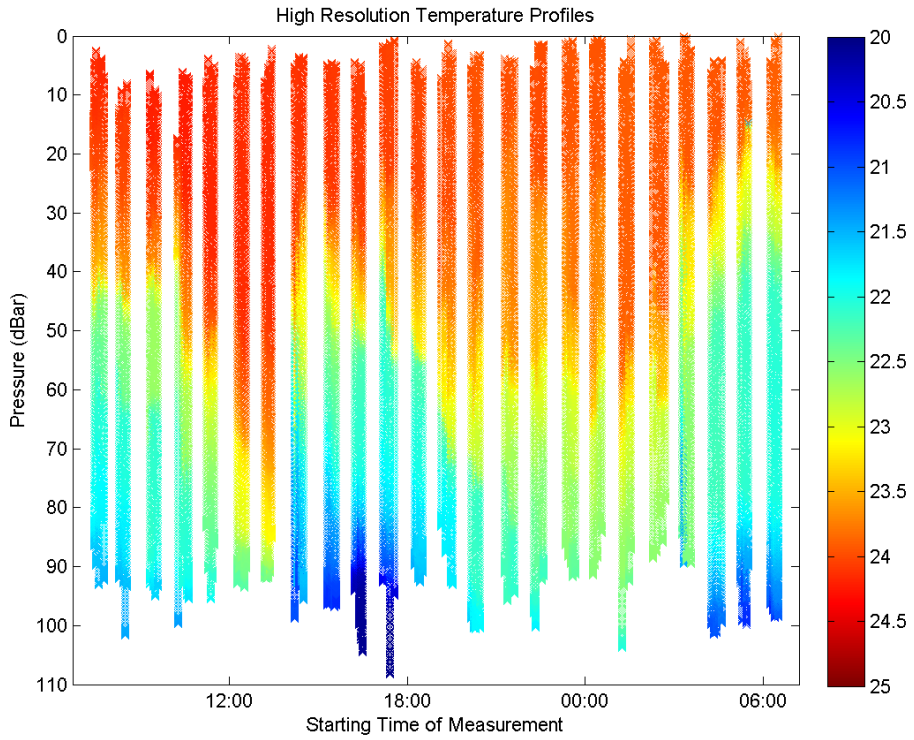

Figure A.3: Temperature measured with the FP07 microstructure probe at 512 Hz.

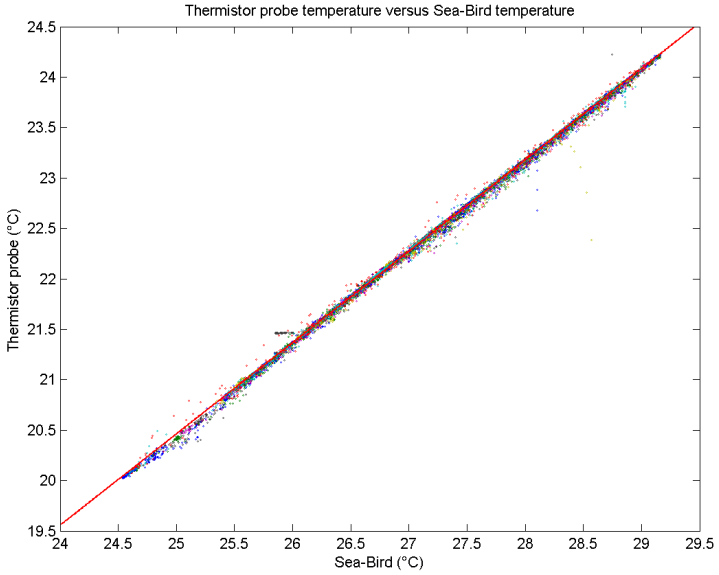

Figure A.4: Temperature measured with the FP07 microstructure probe has an offset with respect to the temperature measured by the Sea-Bird thermometer.

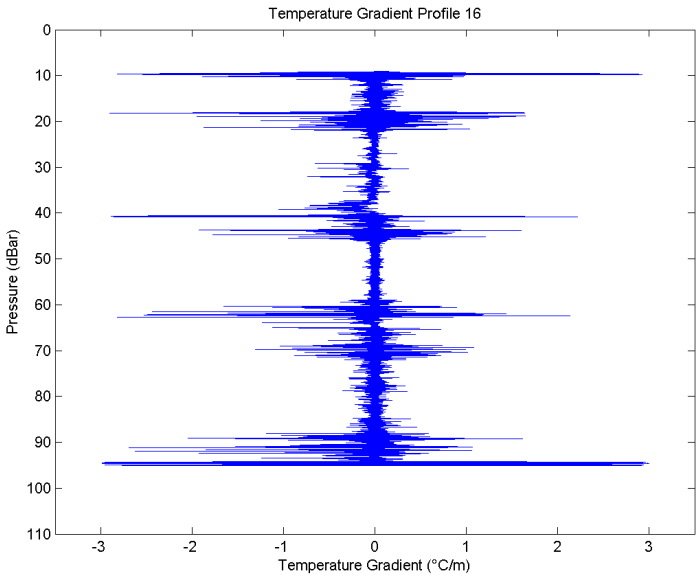

Figure A.5: Temperature gradient of profile number 16.

Appendix B

Drop speed

In this appendix all the histograms made about the drop speed are displayed.

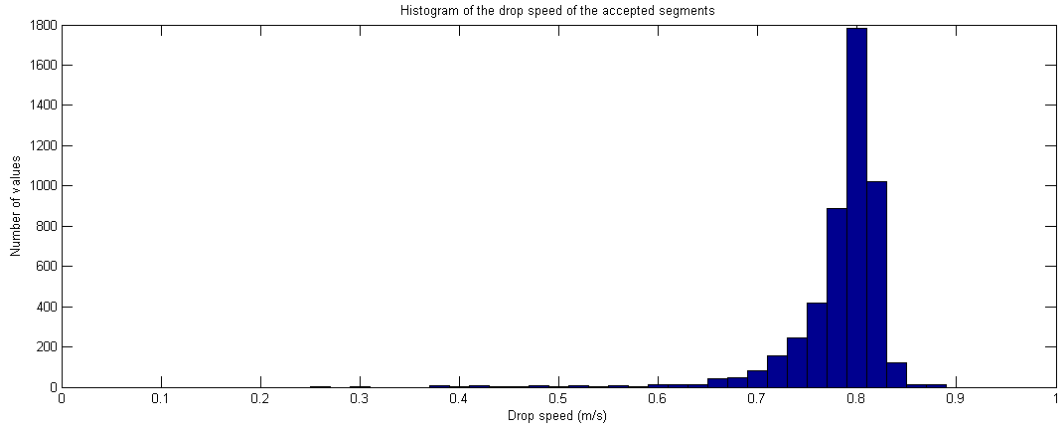

Figure B.1: Histogram of the drop speed of the accepted segments.

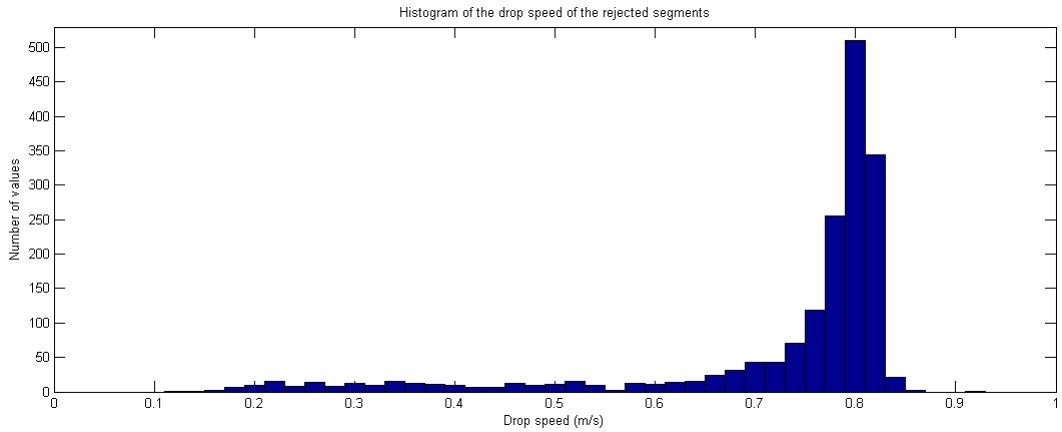

Figure B.2: Histogram of the drop speed of the rejected segments.

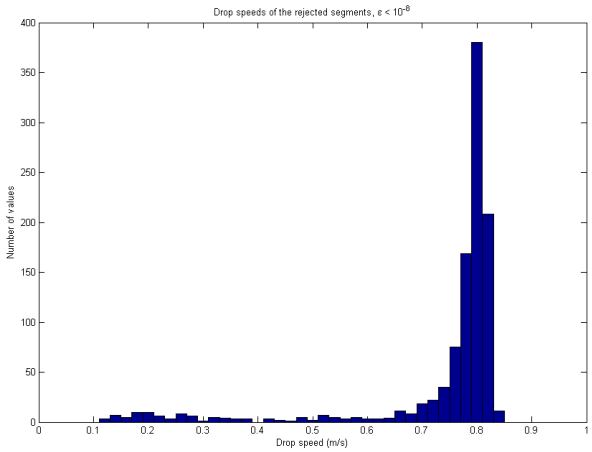

Figure B.3: Histogram of the drop speed of the rejected segments, $\epsilon < 10^{-8}$.

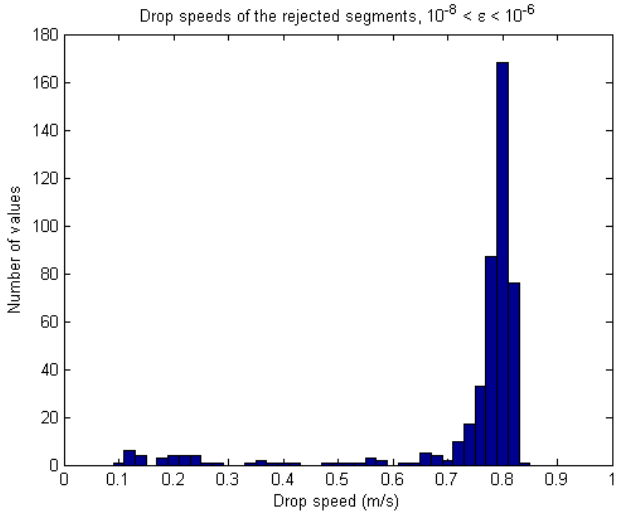

Figure B.4: Histogram of the drop speed of the rejected segments, $10^{-8} < \epsilon < 10^{-6}$.

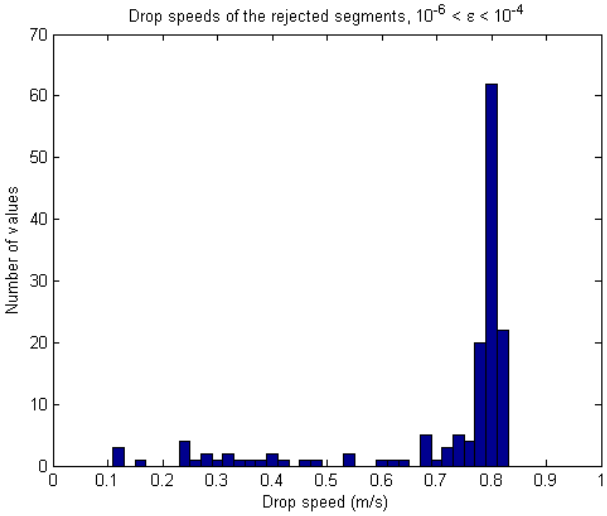

Figure B.5: Histogram of the drop speed of the rejected segments, $10^{-6} < \epsilon < 10^{-4}$.

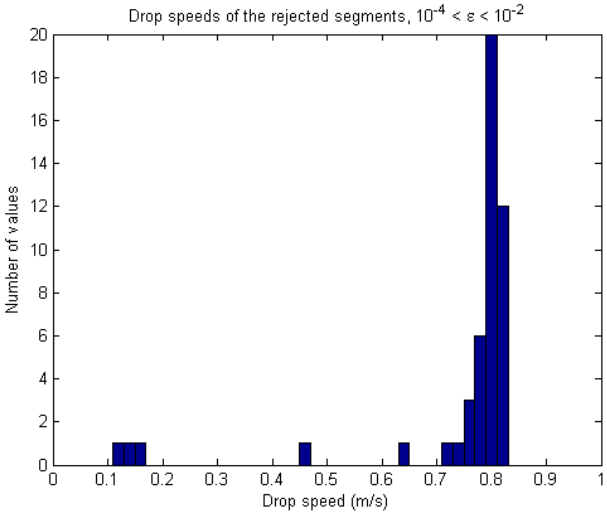

Figure B.6: Histogram of the drop speed of the rejected segments, $10^{-4} < \epsilon < 10^{-2}$.

Appendix C

Results from other locations

In this appendix the results from the other locations (not the 123 casts at BUBS) are presented. There is no visual quality control done on these locations, the data was only run through the program to get some idea of the usefulness of the data.

B.1 Station N100

At this station 11 casts were done on the 8th of April 2011.

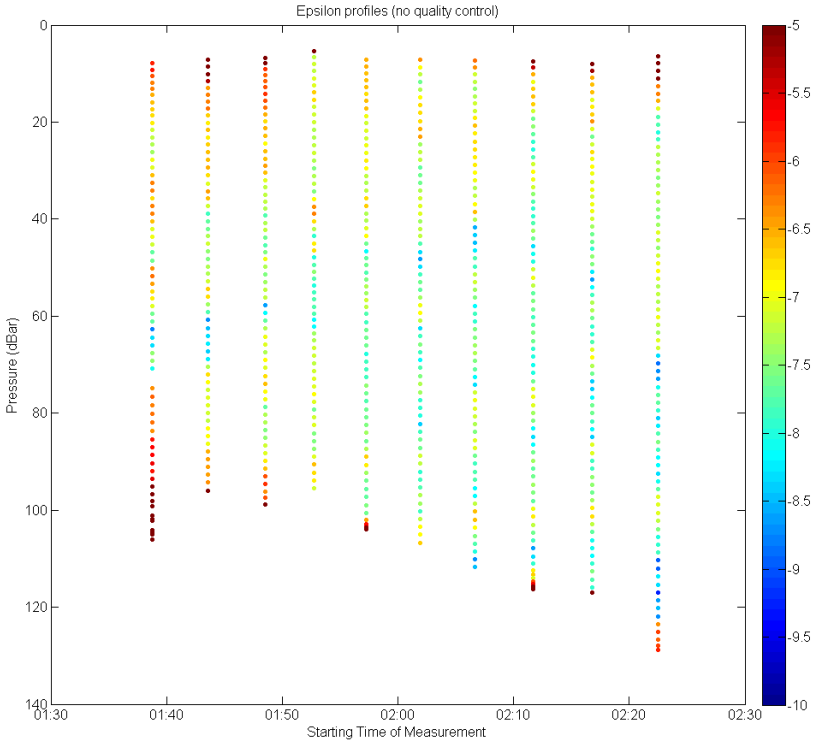

Figure C.1: The ϵ profiles as calculated by the program using the fitting method, without any visual quality control. (latitude,longitude:-21.8480,113.9049)

B.1 Station N50

At this station 10 casts were done on the 8th of April 2011.

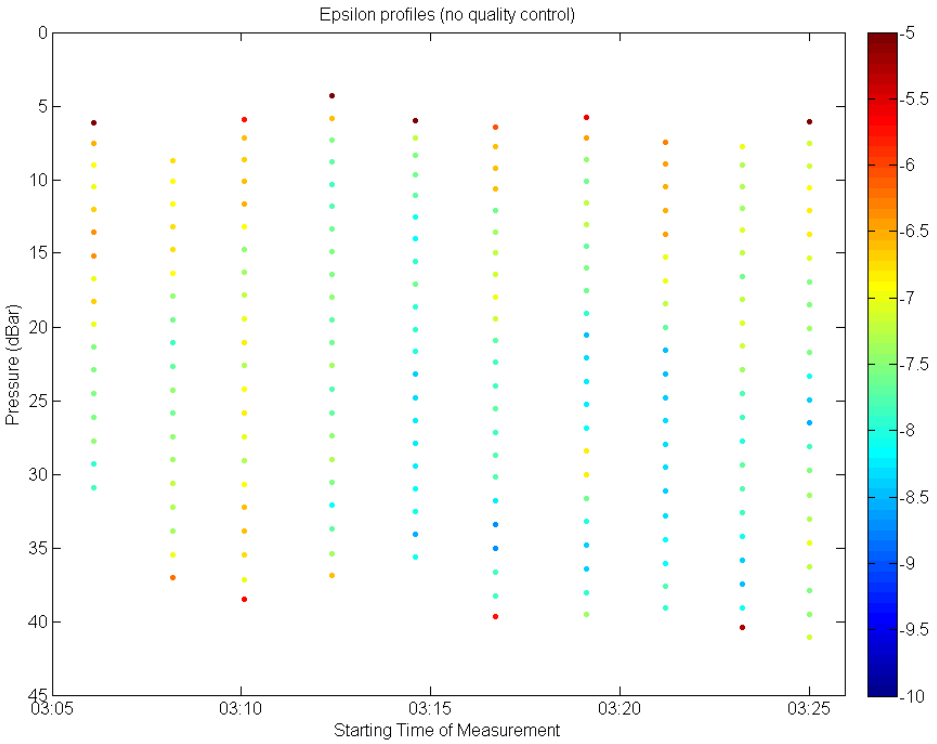

Figure C.2: The ϵ profiles as calculated by the program using the fitting method, without any visual quality control. (latitude,longitude:-21.8668,113.9469)

B.1 Station N1O

At this station 7 casts were tried, but only 5 were successful. They were done on the 8th of April 2011.

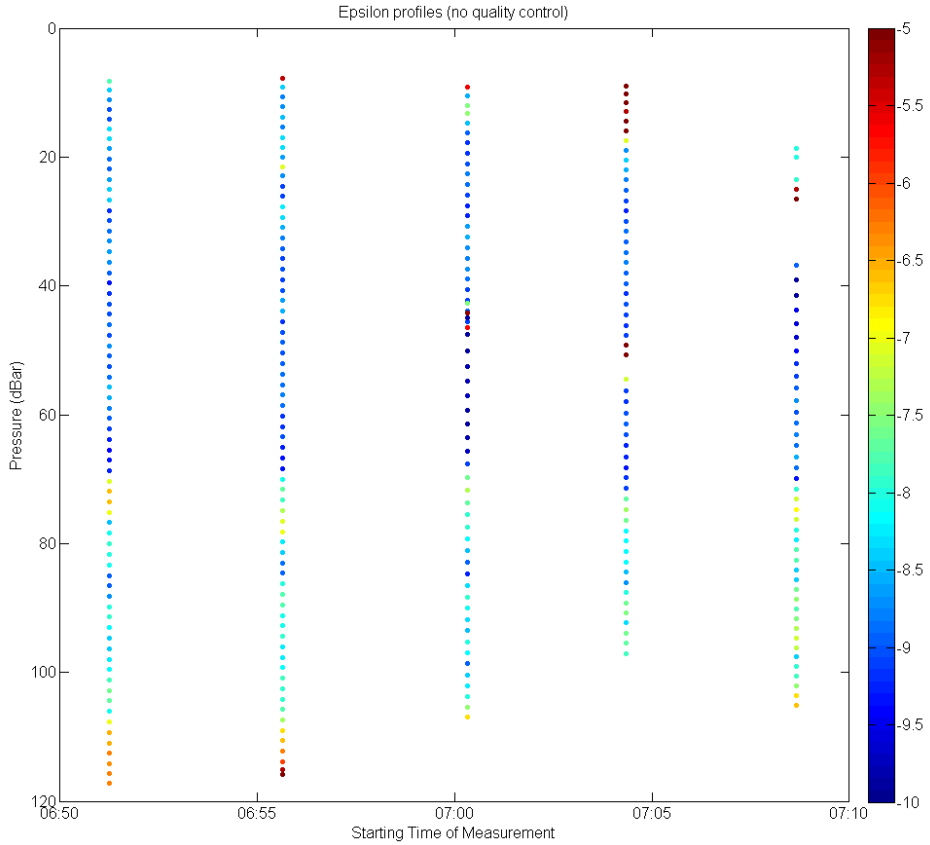

Figure C.3: The ϵ profiles as calculated by the program using the fitting method, without any visual quality control. (latitude,longitude:-21.6900,114.0621)

B.1 Station N1C

At this station 11 casts were tried, but only 10 were successful. They were done on the 8th of April 2011.

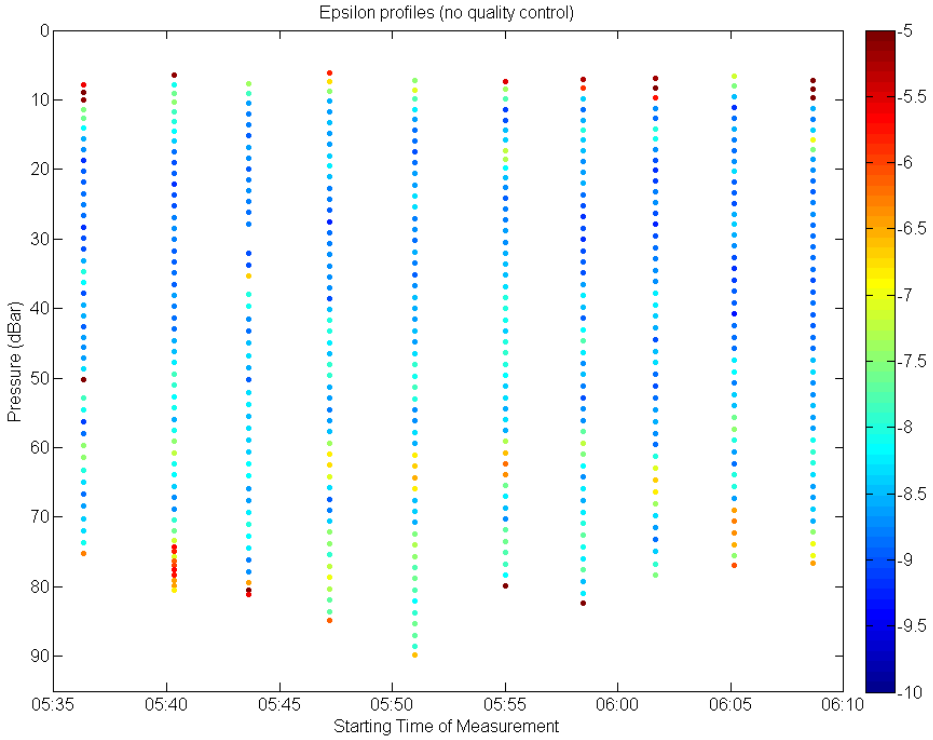

Figure C.4: The ϵ profiles as calculated by the program using the fitting method, without any visual quality control. (latitude,longitude:-21.7057,114.0768)

B.1 Station NICOP

On the 7th of April 2011, 109 casts were done, which started at the NICOP station. The path that was taken for the other casts can be seen in figure C.6. Because the path is moving inshore, the depth is getting shallower along the way.

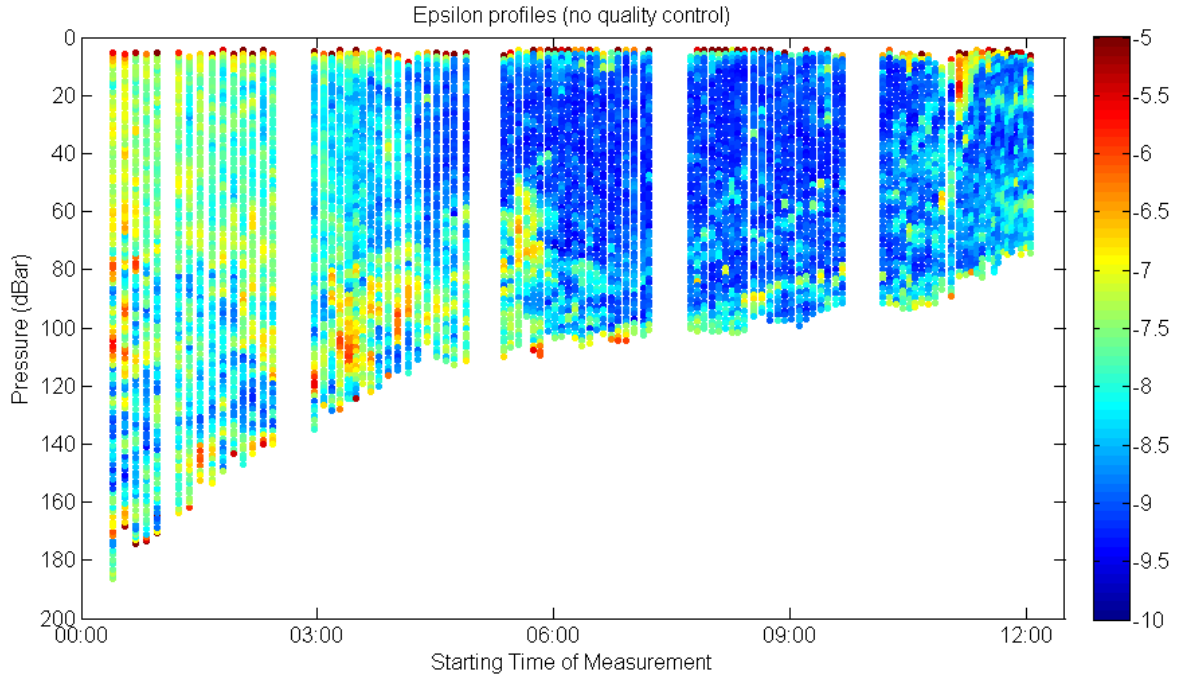

Figure C.5: The ϵ profiles as calculated by the program using the fitting method, without any visual quality control. (latitude,longitude:-21.1188,114.6331)

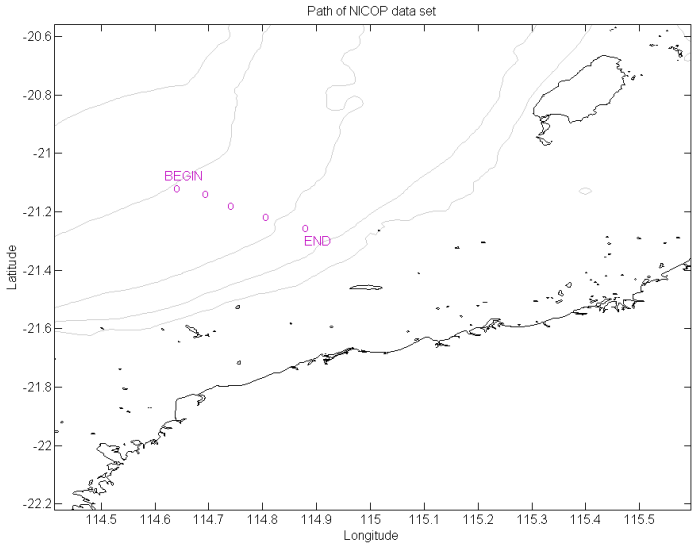

Figure C.6: The path that was taken to take all the 109 casts.

B.1 Station N316

At this station 5 casts were done on the 6th of April 2011.

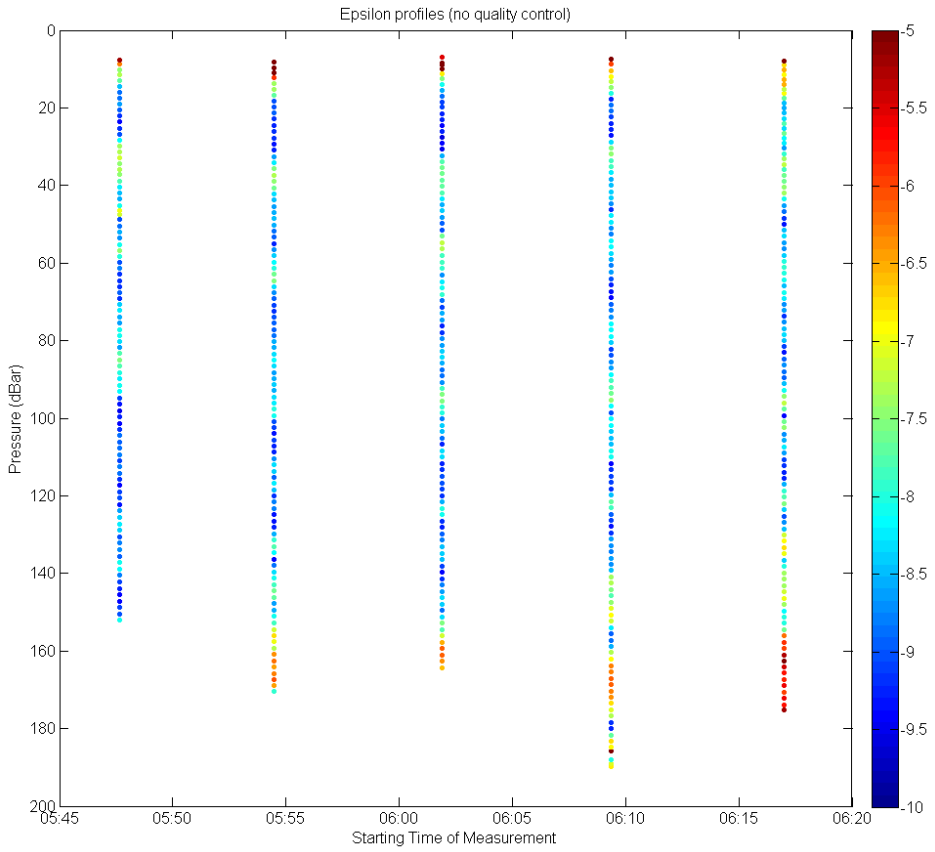

Figure C.7: The ϵ profiles as calculated by the program using the fitting method, without any visual quality control. (latitude,longitude:-20.1096,115.0513)

B.1 Station N3O

At this station 5 casts were done on the 6th of April 2011.

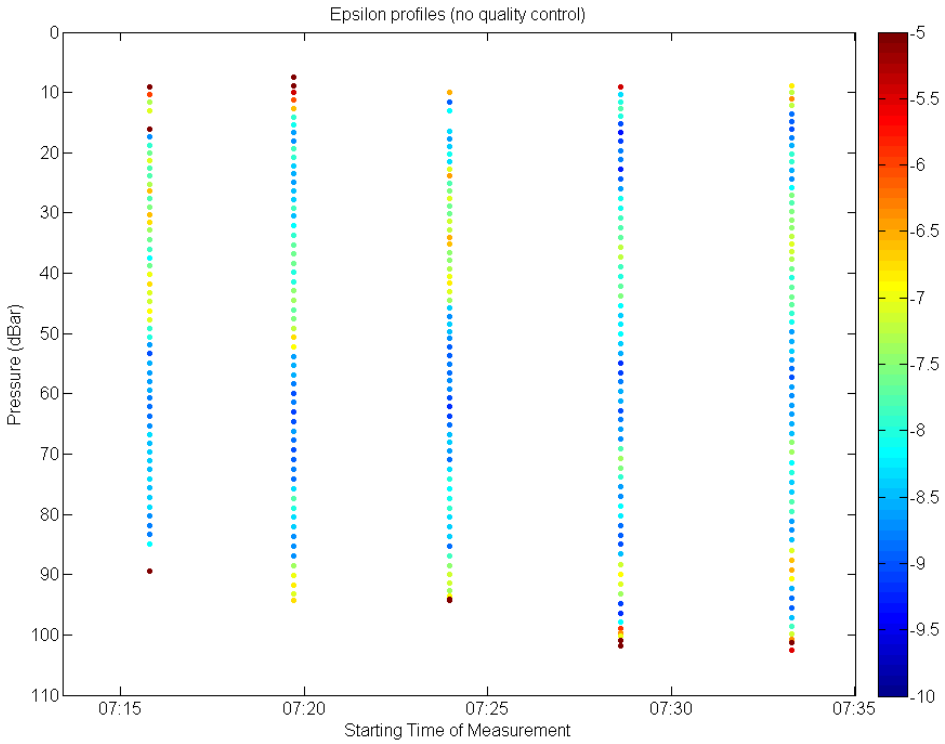

Figure C.8: The ϵ profiles as calculated by the program using the fitting method, without any visual quality control. (latitude,longitude:-20.1574,115.1278)

B.1 Station N3C

At this station 5 casts were done on the 6th of April 2011.

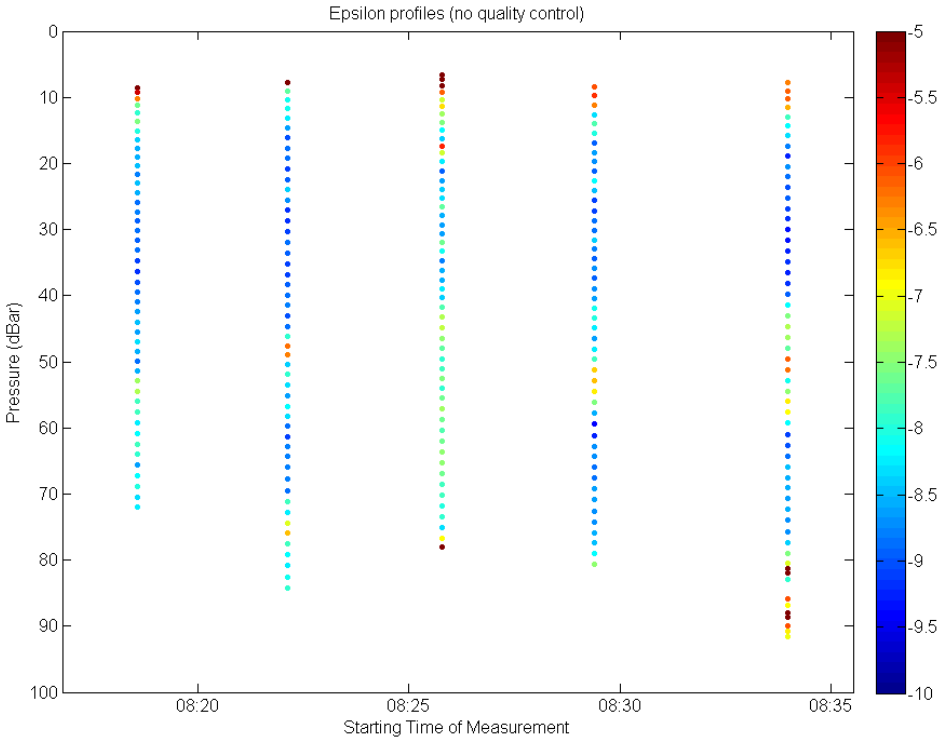

Figure C.9: The ϵ profiles as calculated by the program using the fitting method, without any visual quality control. (latitude,longitude:-20.1858,115.1688)

B.1 Station N3I

At this station 5 casts were done on the 6th of April 2011.

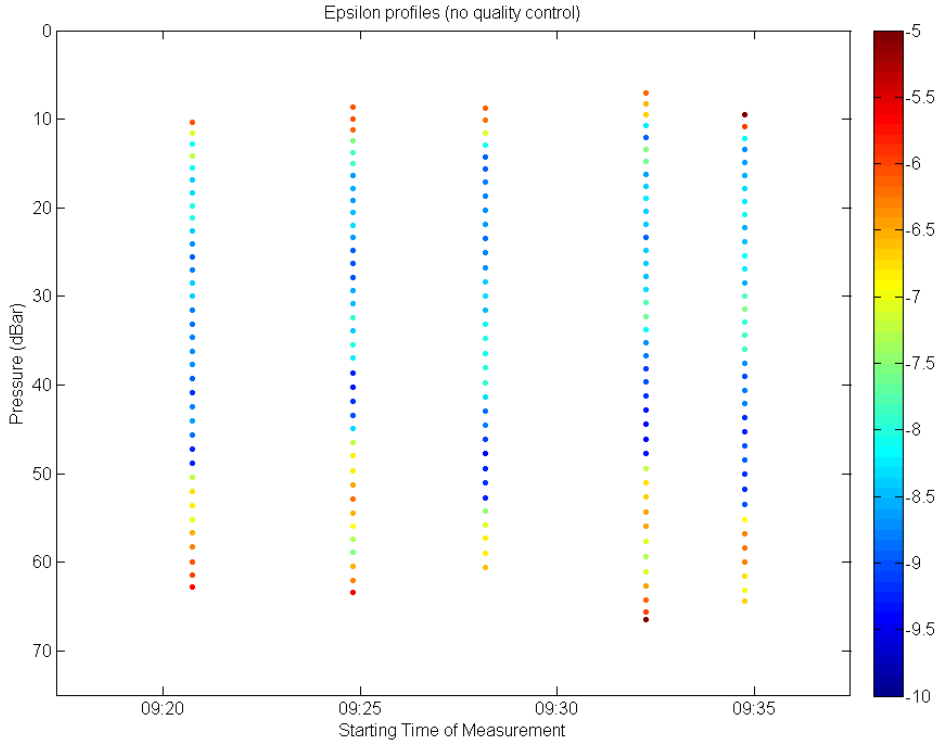

Figure C.10: The ϵ profiles as calculated by the program using the fitting method, without any visual quality control. (latitude,longitude:-20.2228,115.2230)

B.1 Station N317

At this station 5 casts were done on the 6th of April 2011.

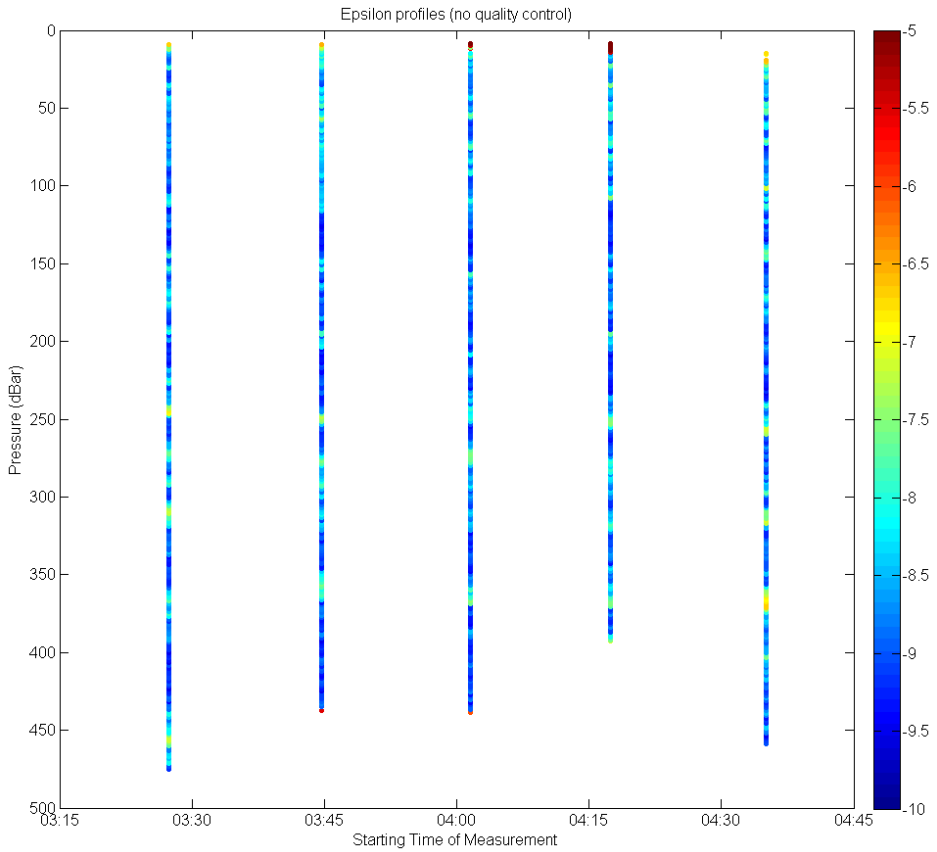

Figure C.11: The ϵ profiles as calculated by the program using the fitting method, without any visual quality control. (latitude,longitude:-20.0686,115.3099)

B.1 Station PIL200

At this station 10 casts were done on the 5th of April 2011.

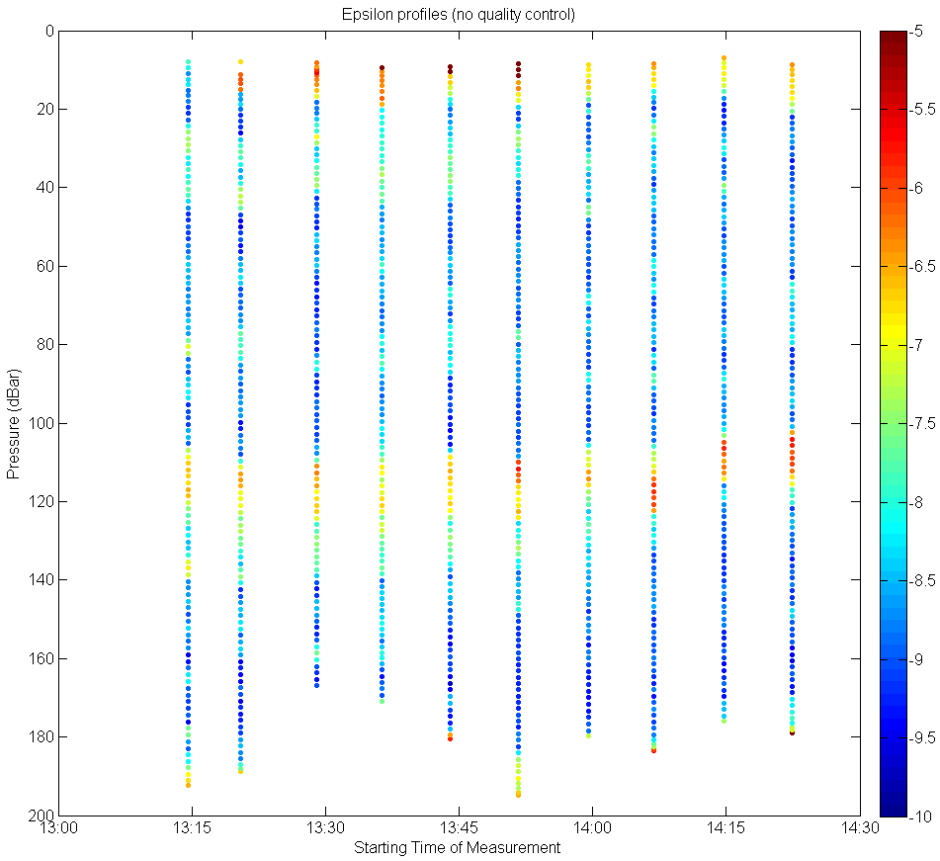

Figure C.12: The ϵ profiles as calculated by the program using the fitting method, without any visual quality control. (latitude,longitude:-19.4383,115.9144)

B.1 Station N4L

At this station 7 casts were done on the 5th of April 2011, but the first casts was not successful.

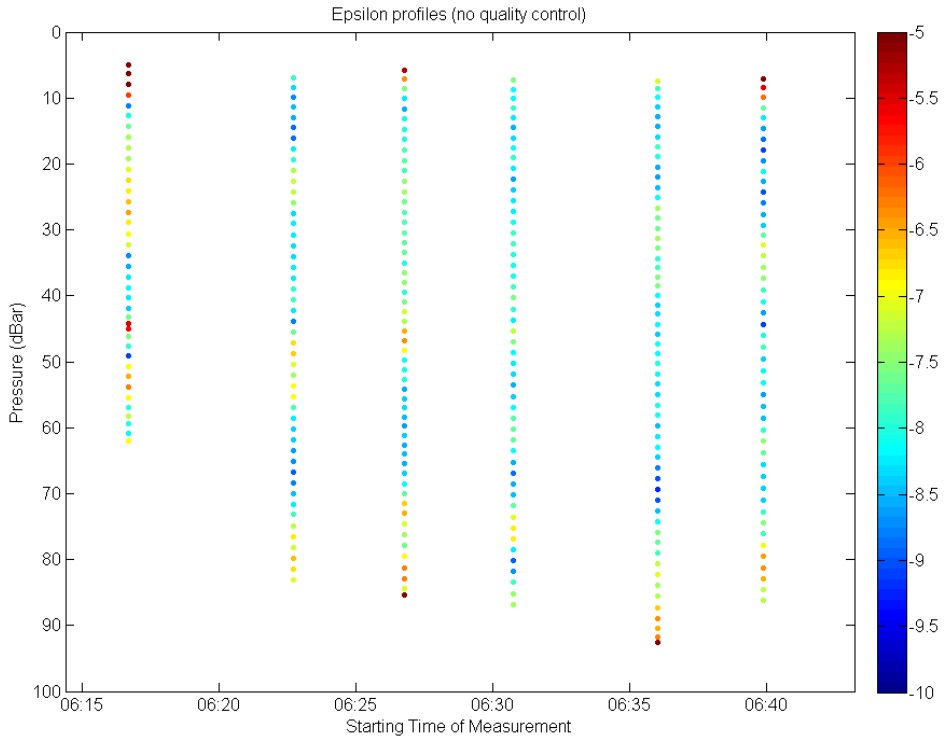

Figure C.13: The ϵ profiles as calculated by the program using the fitting method, without any visual quality control. (latitude,longitude:-19.7452,116.0004)

B.1 Station N4O

At this station 5 casts were done on the 5th of April 2011.

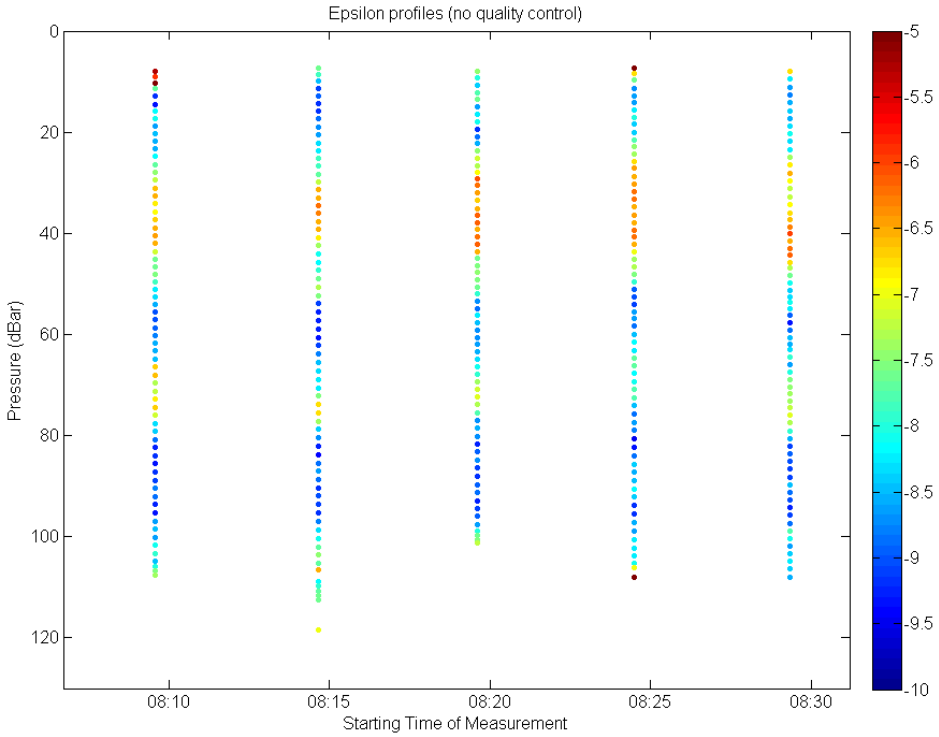

Figure C.14: The ϵ profiles as calculated by the program using the fitting method, without any visual quality control. (latitude,longitude:-19.6182,116.0271)

B.1 Station N4B

At this station 10 casts were done on the 10th of April 2011.

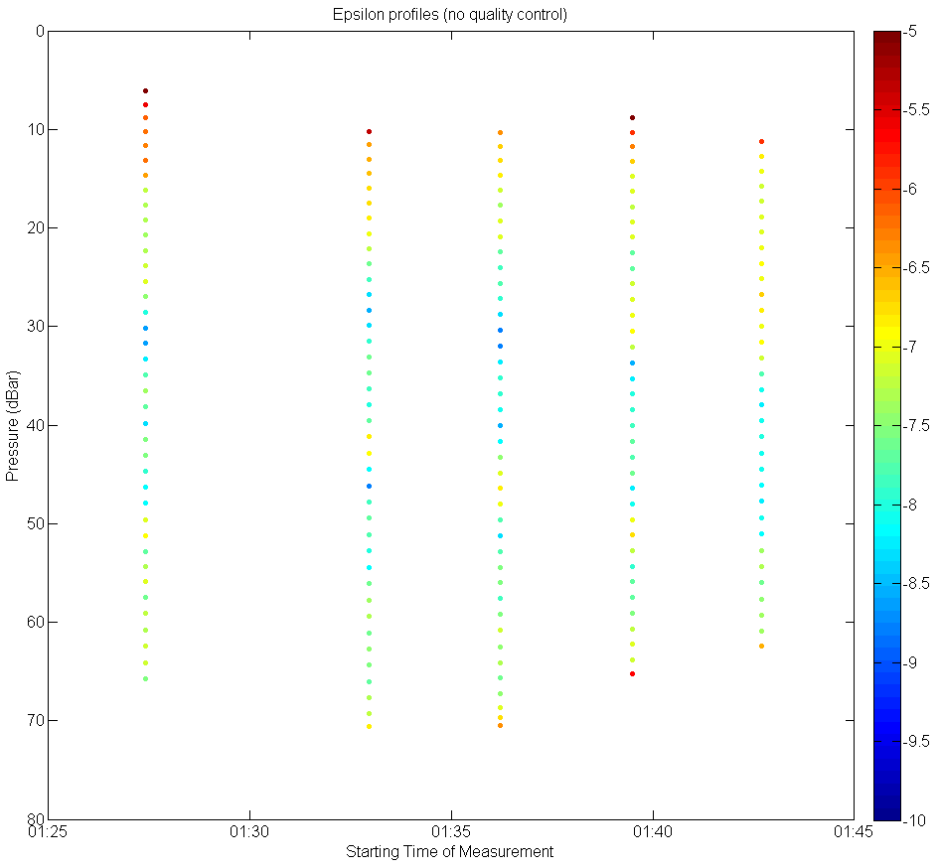

Figure C.15: The ϵ profiles as calculated by the program using the fitting method, without any visual quality control. (latitude,longitude:-19.7484,116.0677)

B.1 Station BUBS

At this station 123 casts were done on the 10th and 11th of April 2011, which are discussed in the main part of this report. A few days earlier there were also 12 casts done on the 5th of April.

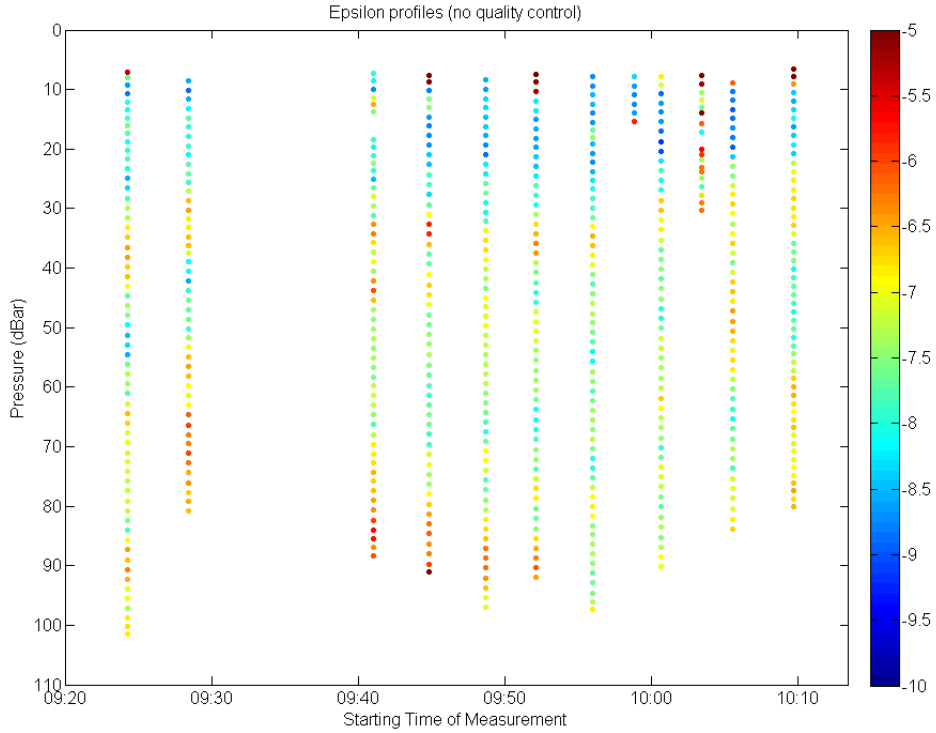

Figure C.16: The ϵ profiles as calculated by the program using the fitting method, without any visual quality control. (latitude,longitude:-19.6667,116.0833)